International Journal of Thermal Sciences 196 (2024) 108738

Contents lists available at ScienceDirect

International Journal of Thermal Sciences

journal homepage: www.elsevier.com/locate/ijts

Investigation of surface inclination effect during dropwise condensation of flowing saturated steam

Marco Tancon, Antonio Abbatecola, Matteo Mirafiori, Stefano Bortolin, Elena Colusso, Alessandro Martucci, Davide Del Col *

Department of Industrial Engineering, University of Padova, Via Venezia 1, 35131, Padova, Italy

ARTICLE INFO

Keywords:
Dropwise condensation
Vapor velocity
Surface inclination
Heat transfer
Droplet population
Modeling

ABSTRACT

When a pure vapor condenses over a surface, it can form a continuous liquid film or a multitude of discrete droplets, thus realizing the so-called dropwise condensation (DWC). In the literature, most of the experimental data refer to DWC on vertical condensing surfaces with quiescent vapor. However, in many applications, the condensing vapor usually has a non-zero flow velocity with a consequent effect on the sliding motion of droplets. Moreover, the drag force due to vapor velocity may be the only mechanism for liquid removal on a horizontal surface or in space applications. A systematic investigation of the effects of vapor drag and surface inclination on the heat transfer and droplet population during DWC is needed and is addressed in the present paper.

Here, DWC of flowing steam is experimentally studied on sol-gel silica-based coated aluminium substrates at three different inclinations: vertical, inclined at 45°, and horizontal. Heat transfer coefficient (HTC) and droplet population measurements are performed in a wide range of heat flux (260–610 kW m^{-2}) and average vapor velocity (3.3–13.8 m s^{-1}). When decreasing the tilt angle, from vertical to horizontal, due to the lower contribution of the gravity force, the average droplet size increases, and a strong HTC reduction is observed above all at low vapor velocities. Because of the vapor drag force, the HTC increases with steam velocity and, at the highest mass velocity, the HTC is independent from the surface inclination. A model for the droplet departing radius in the presence of vapor velocity, initially proposed by the present authors for the sole case of vertical surfaces, is here modified to account also for the effect of surface inclination and then assessed against the present experimental data. Hence, we propose to predict the heat flux during DWC by coupling the new equation for the departing radius with the available models of heat transfer through a single droplet and drop-size distribution. The developed calculation method is found to provide satisfactory predictions of the HTC for the whole range of vapor velocity, heat flux and surface inclination.

1. Introduction

In recent years, the global community has become increasingly aware of the urgent need to address the challenges posed by climate change. Researchers around the world are at the forefront of this effort, working to develop innovative solutions to mitigate the impact of human activities on the environment. Depending on the application, different strategies are being investigated, aiming both at replacing currently used working fluids with others having a lower environmental impact and at improving the efficiency of thermal processes [1–3]. In the case of steam condensation, the promotion of dropwise condensation (DWC) instead of traditional filmwise condensation (FWC) has been identified as a viable strategy for the enhancement of the two-phase heat transfer. Dropwise condensation is a quasi-cyclic process that involves droplets nucleation, direct condensation-induced growth, coalescence-driven growth until the departing size, and finally surface renewal through droplet sliding [4]. Since the DWC process involves the presence of discrete drops rather than a continuous liquid film, it allows to achieve heat transfer coefficients (HTC) 5–9 times higher compared to FWC [5,6]. A more efficient condensation mechanism would result in economic and environmental benefits to many industrial applications [7–9]. However, the major challenge for real-life applications remains the durability of such coatings under severe environmental conditions (i.e. scratching, corrosion, fouling or high thermal stresses) [10,11].

The literature agrees that the heat transfer during dropwise condensation depends on the heat exchanged by each droplet and on the

* Corresponding author.
E-mail address: davide.delcol@unipd.it (D. Del Col).

https://doi.org/10.1016/j.ijthermalsci.2023.108738
Received 18 July 2023; Received in revised form 15 September 2023; Accepted 24 October 2023
Available online 7 November 2023

distribution of drop-size on the condensing surface [4,12]. As stated in Refs. [13–15], the efficiency of DWC process can be enhanced by reducing the average droplet dimension. In particular, to improve the condensation HTC, strategies for the reduction of the departing radius (which is the result of a force balance between adhesion, gravity and drag forces) should be pursued. In ground applications, the departing radius (r_{max}) can be reduced by decreasing the adhesion force (which sticks the drop to the surface) or increasing the gravity and drag forces (which induce droplet movement). The gravity force component responsible of droplet motion depends on the inclination of the condensing surface, while the drag force is dependent on the vapor velocity. On the other hand, the adhesion force can be reduced by decreasing the wettability of the surface (specifically the contact angle hysteresis). In the literature, most of the studies are focused on DWC of pure steam under quiescent vapor conditions and only few works explore the effect of vapor velocity on the dropwise condensation phenomenon. Similarly, the number of studies dealing with the effect of the inclination of the condensing surface is even lower. For the best of the authors' knowledge, no study faces the coupled effect of surface inclination and vapor velocity during DWC of pure steam.

Regarding the effect of vapor velocity during DWC, the literature shows that an increase of steam velocity leads to a decrease of droplet departing radius and an increase of HTC [16–18]. Recently, Tancon et al. [19,20] made steps forward in understanding the effect of vapor velocity on DWC by experimentally investigating DWC of steam at varying average inlet vapor velocity (v_v = 3–15.5 m s^{-1}) on vertical substrates. In addition to the experimental work, the authors proposed a calculation method to account for the heat transfer coefficient increase due to vapor velocity.

For what concerns the effect of surface inclination on DWC, the few measurements available in the literature refer to almost negligible vapor velocity. Leipertz and Fröba [21] performed tests on a copper disc for tilt angles of the condensing surface from 30° to 180° (where 0° corresponds to a horizontal substrate with DWC occurring on the top side, while 180° to a horizontal surface with DWC occurring on the bottom side). The results showed that the HTC deceased by 17 % when the surface inclination angle varied from 90° to 30°, while the reduction of HTC was much higher (about 55 %) when the angle varied from 90° to 180°. Citakoglu and Rose [22] performed measurements during DWC of pure water vapor on a copper plate functionalized by dioctadecyl disulphide. The authors investigated the variation of the steam-side HTC by varying the tilt angle of the condensing surface from upward to downward orientation. With regards to the horizontal upward facing surface, it was observed a HTC reduction by about 60 % compared to the vertical configuration. Similar results were found also for the horizontal downward facing surface. Bonner [23] investigated dropwise condensation of pure steam on surface with graded hydrophobicity. Different inclinations of the condensing surface were considered: vertical downward, 45° inclined (aided by gravity), horizontal and 5° inclined upward. For a fixed heat flux of 300 kW m^{-2}, the results show a reduction in the HTC by around 70 % when varying the surface inclination from vertical to horizontal. It is important to note that none of those studies has ever investigated the effect of surface inclination at varying vapor velocity.

Although the study of DWC on horizontal surfaces (thus without the contribution of gravity to droplet removal) may be of less interest for ground application (for which the vertical orientation of the condensing surfaces is to be preferred), it is fundamental for space applications but also for the comprehension of drop removal mechanisms. In fact, understanding the effect of gravity in ground environment can be a first step in the investigation of DWC under microgravity conditions. In the available literature, very few works deal with the condensation phenomena in microgravity conditions [24–26]. In particular, regarding dropwise condensation under microgravity conditions, previous research has only partially explored droplet dynamics [27], while the heat transfer performance during DWC has not been addressed at all.

The present work aims to fill a gap regarding the knowledge of vapor velocity and surface inclination combined effects on heat transfer and droplet population during dropwise condensation of pure water vapor. An aluminium sol-gel coated sample is here considered as modified wettability surface on which condensation takes place. Heat transfer coefficient data have been collected considering three different surface inclinations (vertical downflow, inclined at 45° downward, and horizontal), varying the average inlet vapor velocity (between 3.3 m s^{-1} and 13.8 m s^{-1}) while keeping a constant heat flux (about 400 kW m^{-2}). In support of the thermal measurements, flow visualizations have been performed using a high-speed camera to map the droplet population on the condensing surface, providing insights into the drop-size distribution, departing radius and characteristic renewal time. The present experimental results have been used to extend the model proposed by Tancon et al. [19] to the case of non-vertically oriented condensing surfaces. We show that, putting together the new equation developed for the prediction of departing droplet radius with available models for drop-size distribution and heat transfer through a single droplet, it is possible to determine the DWC heat transfer coefficient even in presence of non-negligible steam velocity and with different tilt angles of the surface.

2. Description of surface characteristics and experimental technique

2.1. Surface fabrication and characterization

Aluminium sol-gel coated substrates are used to investigate the combined effect of vapor velocity and surface inclination during DWC of steam. The substrate used for the condensation tests was high purity aluminium sample (AW 1050, minimum aluminium content 99.50 %), mirror-polished on the condensation surface (50 mm × 20 mm) before coating deposition. The procedure used to fabricate the sol-gel coating (hereinafter called P7M3) is fully described in Parin et al. [28] and additional information that includes also surface characterization methods is reported in Supplementary Material (S1). This sol-gel coating was identified as a good solution to ensure adequate robustness in such harsh environments characterized by high heat flux, high temperature and high vapor velocity [28].

The thickness (δ_{HC}) of the investigated coating, evaluated by ellipsometry (Supplementary Material S2), was 400 ± 25 nm. Assuming a thermal conductivity of 0.2 W m^{-1} K^{-1} (as reported in the literature for similar coatings [29]), the thermal resistance per unit area of the coating is about 2 m^2 K MW^{-1}.

Contact angles were determined considering the averaged value of nine measurements performed on nine different locations on the sample (more information is provided in Supplementary Material S3); the standard deviation is also considered as an indicator of the uniformity of contact angles on the investigated surface. After coating deposition, the wettability behaviour was similar for all the developed samples, with an advancing contact angle $\theta_a = 87° \pm 2°$ and a receding contact angle $\theta_r = 64° \pm 5°$. Therefore, since the equilibrium contact angle is smaller than 90°, the developed surfaces can be classified as hydrophilic with reduced contact angle hysteresis compared to the baseline aluminium ($\theta_a \approx 60°$, $\theta_r \approx 0°$) [4]. Although hydrophilic, the developed samples were found to promote and sustain DWC. As experimentally observed by several authors [12,30], in order to achieve stable dropwise condensation, the low contact angle hysteresis of the surface is more important than its intrinsic wettability (which is usually associated with the equilibrium contact angle). It is worth noting that dropwise condensation on hydrophilic surfaces presents further advantages such as lower thermal resistance associated with conduction through the droplets, enhanced droplets nucleation and therefore higher heat transfer coefficients [5].

Since the interaction with water at high temperature can lead to the degradation of the hybrid silica sol-gel coatings [10], wettability and coating thickness measurements were also performed at the end of the

heat transfer tests. After condensation tests, the film thickness slightly decreased by about 20 nm and the contact angles remained almost the same ($\theta_a = 88° \pm 3°$ and $\theta_r = 61° \pm 6°$). Such modest variations in coating thickness and surface wettability were not expected to affect the heat transfer and the droplet population measurements presented in the following Sections.

2.2. Experimental test rig for DWC measurements and data reduction procedure

Condensation tests were carried out using the test rig described in Tancon et al. [20]. The experimental apparatus is a thermosiphon loop, schematically shown in Fig. 1. The vapor produced in the boiling chamber (BC) flows by natural circulation into the condensation test section which includes the 50 mm × 20 mm aluminium sample. The design of the test section, with a glass window on one side, allows simultaneous measurement of heat transfer coefficients and visualization of the droplets population. More details about the optical system for droplets observation and the experimental facility are provided in Supplementary Material S4 and S5, respectively.

In order to investigate the DWC phenomenon when varying the surface inclination, the apparatus described in Refs. [20,31] was modified to allow for different inclinations of the test section and thus of the condensing surface. In particular, part of the pipelines before and after the test section were modified to change the tilt angle of the test section. In this work, the tilt angle of the surface (β) is defined as the angle between the horizontal plane and the plane containing the condensing surface. According to this definition, three different orientations were addressed in the present study: vertical $\beta = 90°$ (gravity and vapor flow act in the same direction), inclined at $\beta = 45°$ (gravity vector and vapor flow form an angle of 45°), and horizontal $\beta = 0°$ (gravity perpendicular to vapor flow). By varying the inclination of the condensing surface, the contribution of the gravity force to droplet removal can be changed. In fact, when the surface is vertical, gravity acts in the same direction as the vapor flow, favouring the removal of the condensate. On the other hand, when the surface is horizontal, the condensate removal is only due to the action of vapor flow.

Inside the test section (Fig. 2b), the vapor flows over the coated surface of the sample and condenses thus rejecting the latent heat to the cooling water flowing in counter-current. Water temperature and flow rate are controlled by a thermostatic bath (TB1). The temperature difference between the cooling water inlet and outlet is measured by a calibrated three-junction thermopile, while the mass flow rate is measured by a Coriolis-effect flow-meter. The design of the coolant channel allows the cooling water flow on the backside of the metallic specimen to be hydrodynamically fully developed, while the coolant mass flow rate provided by TB1 is kept sufficiently high to limit the cooling water temperature increase to around 1 K. Since the leading thermal resistance is on the cooling water side, an almost constant values of HTC and temperature on the cold side ensure an uniform heat flux along the length of the sample.

The specimen is equipped with six T-type thermocouples, three on each side, arranged in pairs. Therefore, for a given axial x position along the sample, the wall temperature is measured at two depths from the surface over which vapor condenses ($z_1 = 1.3$ mm and $z_2 = 2.8$ mm).

To evaluate the heat transfer coefficient during DWC, it is necessary to determine the heat flux exchanged through the sample and the temperature difference between the saturated steam and the substrate (degree of subcooling). The average heat flux transferred through the condensing surface (A) is obtained from the thermal balance on the coolant side of the test section, which can be expressed as:

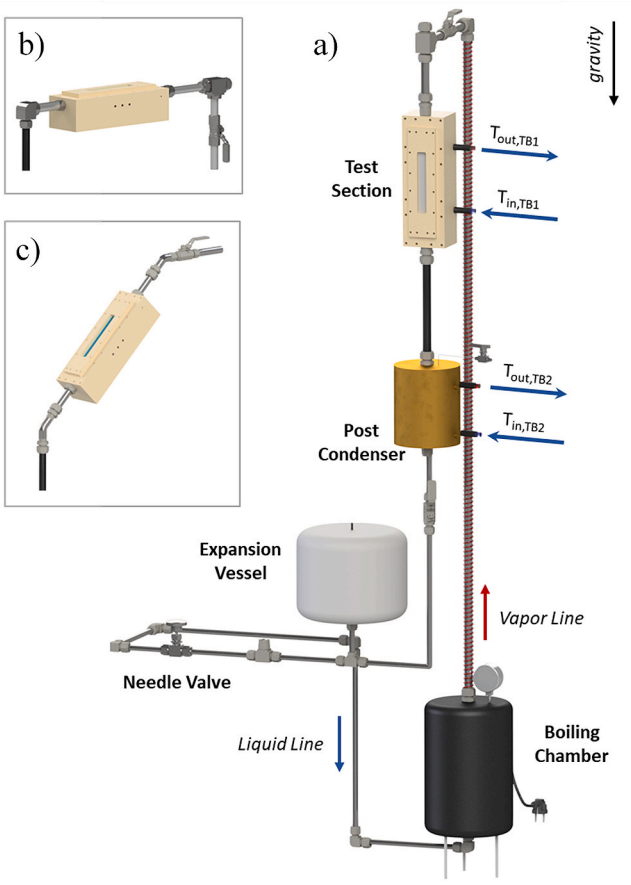

Fig. 1. a) Layout of the experimental apparatus (with the test section vertically mounted) showing the positions of the main components. The other two configurations are also depicted: b) horizontal test section and c) test section inclined at 45°.

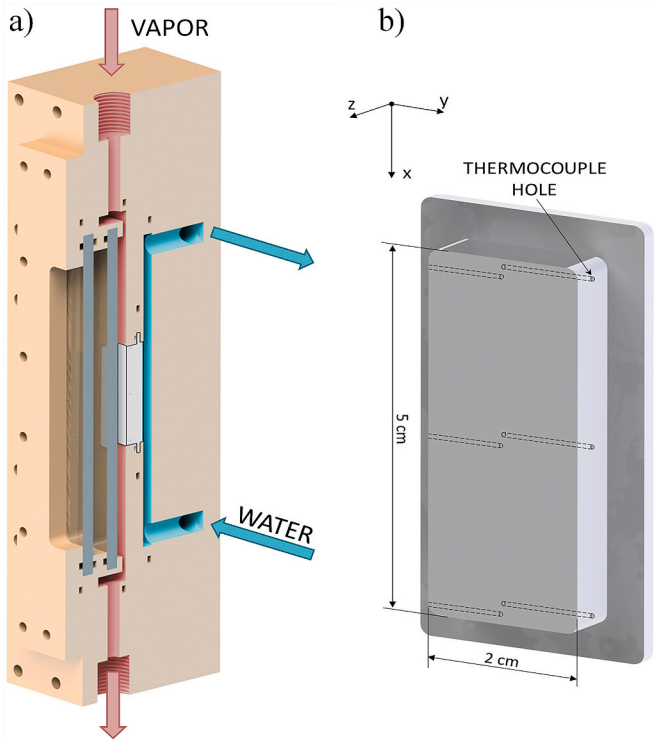

Fig. 2. a) Cross-sectional view of the test section showing the direction of the vapor and cooling water flows; b) 3D model of the tested sample with position of the thermocouples.

$$q = \frac{\dot{m}_w \, c_w \, \Delta T_w}{A} \tag{1}$$

where ΔT_w is the temperature increase of the water in the test section, $\dot{m}_w$ is the cooling water mass flow rate and c_w is the water specific heat. As additional check, the heat flux given by Eq. (1) is compared with the local heat flux measurements (q_i) obtained by applying the Fourier's law to the three pairs of thermocouples inserted in the sample at the two different depths z_1 and z_2 ($T_{z_1,i}$ and $T_{z_2,i}$, respectively):

$$q_i = \lambda_{al} \frac{T_{z_1,i} - T_{z_2,i}}{z_2 - z_1} \tag{2}$$

where λ_{al} is the thermal conductivity of the aluminium, while the i-subscript refers to the longitudinal position along the sample (inlet, middle and outlet). By comparing the heat flux obtained by the energy balance on the water side (Eq. (1)) and the average value obtained from the Fourier's law, it resulted an agreement within 5 %. A detailed description of this procedure is reported in Refs. [31,32].

By considering the readings of the thermocouples inserted into the sample at depth z_1 and the temperature gradient inside the sample, the local temperature of the surface ($T_{wall,i}$) in correspondence of three x positions along the sample (named as inlet, middle and outlet) can be obtained by applying the Fourier's law as follows:

$$T_{wall,i} = T_{z,i} + q \frac{z_1}{\lambda_{al}} \tag{3}$$

Once the local surface temperatures are known at three different positions along the sample, the arithmetical mean of the difference between the saturation temperature and the wall temperature can be evaluated:

$$\Delta T = \sum_{i=in}^{out} \frac{1}{3} \left(T_{sat} - T_{wall,i} \right)_i \tag{4}$$

where, as described in Tancon et al. [20], the saturation temperature T_{sat} is obtained from the value of saturation pressure measured at the test section inlet. Therefore, the average HTC during DWC is evaluated as:

$$\mathrm{HTC} = \frac{q}{\Delta T} \tag{5}$$

Since the present experimental technique gives the temperature difference between the saturation temperature and the substrate temperature just below the coating, in the HTC calculated by Eq. (5) the effect of the sol-gel coating conduction resistance is also included. The validation of the HTC measurement, which was performed by comparing filmwise condensation measurements against FWC correlations, is reported in Supplementary Material (Sec. S7).

Measuring the electrical power supplied by the electrical resistances within the boiling chamber (Q_{BC}), it is possible to determine the mass flow rate circulating in the thermosyphon ($\dot{m}_v$) as:

$$\dot{m}_v = \frac{Q_{BC}}{h_v - h_{ls}} \tag{6}$$

where the vapor enthalpy (h_v) is evaluated from the saturation pressure, while the enthalpy of the subcooled liquid (h_{ls}) is obtained from the temperature and pressure conditions at the entrance of the boiling chamber. Hence, the mass flux (G_v) of the fluid in the test section can be determined as follows:

$$G_v = \frac{\dot{m}_v}{S_v} \tag{7}$$

where S_v is the cross section of the channel (S_v = 5 mm × 30 mm). Finally, since the test section is fed with dry saturated vapor, the average inlet vapor velocity is obtained from:

$$v_v = \frac{G_v}{\rho_v} \tag{8}$$

where ρ_v is the vapor density at the saturation pressure. Due to partial condensation occurring inside the test section, the fluid exits the test section as wet saturated vapor and the vapor quality ($x_{v,out}$) can be evaluated as:

$$x_{v,out} = \left[\left(h_{vs} - \frac{Q}{\dot{m}_v} \right) - h_l \right] \frac{1}{h_{lv}} \tag{9}$$

where h_{vs} is the superheated vapor enthalpy at the inlet of the test section, $Q = q\,A$ (Eq. (1)), and h_l is the saturated liquid enthalpy. From the knowledge of $x_{v,out}$, assuming that the vapor phase flows alone in the rectangular channel, it is possible to calculate the average outlet vapor velocity ($v_{v,out}$):

$$v_{v,out} = \frac{v_v \, \rho_{v,in} \, x_{v,out}}{\rho_{v,out}} \tag{10}$$

As the vapor quality decreases along the length of the sample due to condensation, the average vapor velocity also decreases, in particular in the case of the lowest power supplied to the boiling chamber (Table 1). Eq. (10) represents the superficial velocity of the vapor phase [33]. While the real vapor velocity inside the test section may vary from place to place due to the presence of an evolving droplet population, the superficial velocity is an easy to calculate and unambiguous quantity that provides a good estimate of the average vapor velocity. All the thermodynamic properties are calculated by means of REFPROP version 10 [34].

Each experimental point presented in this paper was obtained as the average of 480 measurements taken at a frequency of 1 Hz. The main parameters underwent to uncertainty analysis in accordance with the ISO guide [35], considering a coverage factor of $k = 2$ for the evaluation of combined uncertainties. To ensure accurate heat transfer measurements, temperature transducers were calibrated: after calibration the accuracy of the thermocouples is ±0.05 K, while the thermopile has an accuracy of ±0.03 K. Further details about the calibration procedure are reported in the Supplementary Material (Sec. S6). In Table 1, the directly measured quantities with corresponding type B uncertainty and the derived quantities with their expanded uncertainty are reported. For further details regarding the instrumentation, the methods for avoiding non-condensable gases within the test rig, the data reduction technique and the analysis of uncertainties, the reader can refer to Refs. [20,31,36].

3. Heat transfer and droplet population experimental data

In this Section, the results of the experimental campaign to study the effect of surface inclination during DWC are presented. New data are measured varying vapor velocity and heat flux on 45° inclined and horizontally oriented condensing surfaces. The results are compared to the measurements previously obtained for the vertically oriented condensing surface (which is functionalized with the same coating described in Sec. 2.1) by Parin et al. [28] and Tancon et al. [20]. In total, 17 out of the 26 different operating conditions considered in the present work are original experimental data.

3.1. Effects of surface inclination, vapor velocity and heat flux on HTC

Two different sets of condensation tests were run for each surface inclination condition (horizontal, inclined at 45°, vertical) here considered: as a first step, the effect of the heat flux was investigated by varying the coolant temperature (and thus the surface temperature); after, the effect of vapor velocity was studied by changing the electric power supplied to the boiling chamber. All the other input parameters were maintained constant during each test run (Table 1).

Table 1
Range of variation for the main parameters measured during the experimental campaign. Uncertainty values (considering a coverage factor $k = 2$) are also reported.

	Vertical		Inclined		Horizontal		Uncertainty
Surface tilt angle β [°]	90		45		0		
Absolute Pressure [bar]	1.28		1.23		1.28		±0.1 %
Saturation temperature [°C]	107		106		107		±0.5
Coolant mass flow rate [kg s^{-1}]	0.11		0.10		0.10		±1 %
Electrical Power [kW]	0.8	1–4	1	1–4	1	1–4	±0.1 %
Coolant inlet temperature [°C]	10–70	50	10–70	50	10–70	50	±0.05
Vapor mass flux [kg m^{-2} s^{-1}]	2.5	2.5–10.3	2.6	2.5–10.4	2.6	2.5–10.3	±0.07
Avg. inlet vapor velocity [m s^{-1}]	3.1	3.4–13.6	3.5	3.5–13.7	3.4	3.3–13.8	±0.2
Avg. outlet vapor velocity [m s^{-1}]	1.4–2.6	1.9–12	1.3–2.7	1.9–12	1.4–2.6	1.8–12	±0.3
Vapor quality at TS out [−]	0.25–0.65	0.5–0.9	0.3–0.7	0.5–0.9	0.3–0.7	0.5–0.9	±0.05
Heat flux [kW m^{-2}]	290–610	400	250–610	403	280–590	413	±4 %
HTC [kW m^{-2} K^{-1}]	91–96	97–119	85–89	89–114	58–61	60–113	±6 %

The heat transfer measurements when varying heat flux are presented in Fig. 3. The values measured for the three different surface inclinations refer to heat fluxes from 260 to 610 kW m^{-2}, corresponding to a variation of the coolant inlet temperature from 70 °C to 10 °C. To ensure enough vapor to condense even at the highest heat flux, the power supplied to the boiling chamber was set at 1 kW, which corresponds to an average inlet vapor velocity of about 3.5 m s^{-1} (Fig. 3b). Data taken on the vertically oriented surface, which are taken from Ref. [28], refer to a slightly lower average inlet vapor velocity (3.1 m s^{-1}) as the electric power supplied to the boiling chamber was 800 W. The other operating conditions are reported in Table 1. In the investigated range of conditions, the coated samples were able to sustain DWC regardless of surface inclination, with no transition to FWC even in the case of the horizontal condensing surface. In fact, the vapor velocity inside the thermosyphon loop cannot be zero and, therefore, there is always a drag force due to the vapor flow which enables the condensate removal, preventing the flooding of the surface even at the lowest vapor velocity.

As shown in Fig. 3c, the saturation-to-wall temperature difference (ΔT) is found to increase almost linearly with the heat flux and, thus, the HTC remains almost constant in the heat flux range here investigated (Fig. 3a). This result is expected: most authors found constant HTC trend with heat flux during DWC [6,37]. With regards to the vertical inclination of the condensing surface, which is considered as the reference case, the HTC was around 94 kW m^{-2} K^{-1}. When varying the surface inclination from vertical to horizontal, the HTC is reduced: the sample inclined at 45° exhibited HTC values of about 85 kW m^{-2} K^{-1}, while HTCs of about 60 kW m^{-2} K^{-1} were measured on the horizontal surface. Therefore, compared to the values obtained for the reference case, the HTCs measured on the inclined and horizontal specimens were reduced by 10 % and by 40 %, respectively. These results are in good agreement with the literature dealing with DWC on horizontal surfaces at low vapor velocities [21,22]. Considering the same surface wettability ($\theta_a \approx 87°$, $\theta_r \approx 64°$) and coating thickness (≈400 nm), the different values of HTC reported in Fig. 3a can be attributed to the different surface inclination, which determines the contribution of the gravity force on droplets removal. When the surface is vertically oriented, the component of the gravity force parallel to the flow is maximum: both the gravity and drag forces contribute to the condensate removal. Instead, when the surface is horizontally oriented, the component of the gravity force parallel to the flow is zero: only the vapor drag force contributes to the condensate removal. Consequently, compared to the vertical surface, the drops on the horizontal surface grow to a larger size before sliding and the sliding velocity is reduced, penalizing the efficiency of the DWC mechanism (see the discussion in Sec. 3.3).

It may be interesting to compare these data to the case of filmwise condensation. Even for the horizontal surface at the maximum heat flux, the wall subcooling (defined as the difference between the saturation temperature and the surface temperature) is around 10 K and, therefore, the HTC is around 60 kW m^{-2} K^{-1}. Just for comparison, to achieve a similar heat flux (≈600 kW m^{-2}) during FWC on a vertically oriented surface, the FWC model described in Ref. [31] would require a wall subcooling of about 50 K as input and would predict average HTC values along the condensing surface length of about 12 kW m^{-2} K^{-1}. Therefore, in the range of heat flux 260–610 kW m^{-2}, the HTCs measured on the horizontal surface are 4–5 times higher compared to the values obtained during FWC on a vertical surface. The advantage of promoting DWC instead of FWC increases when considering the dropwise phenomenon

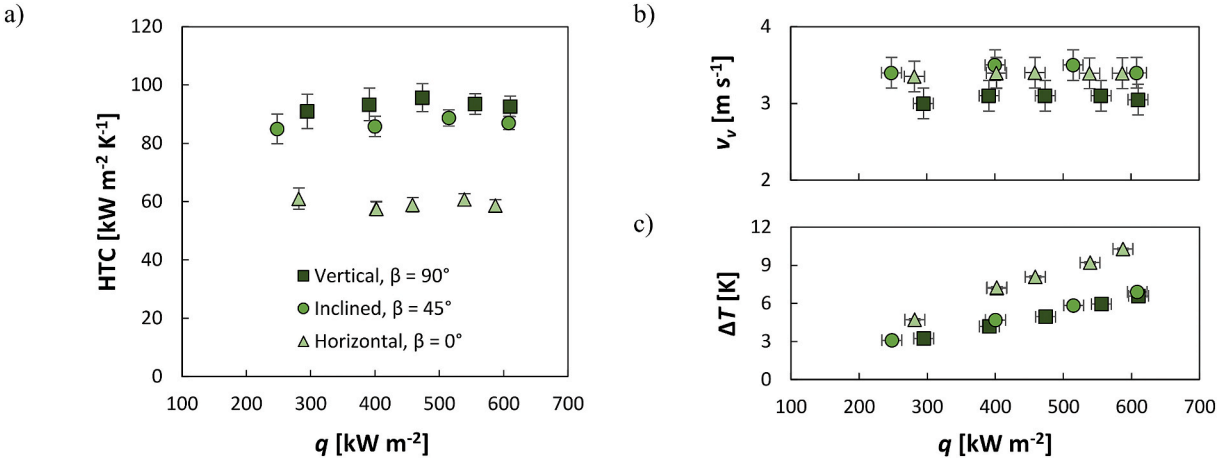

Fig. 3. Heat transfer measurements during DWC of steam when varying heat flux (250–600 kW m^{-2}) for different inclinations of the condensing surface: vertical ($\beta = 90°$), inclined ($\beta = 45°$) and horizontal ($\beta = 0°$). (a) Heat transfer coefficient HTC, (b) average inlet vapor velocity v_v and (c) wall subcooling ΔT versus heat flux q. Values for the vertical configuration are taken from Parin et al. [28].

on the vertical surface: the values of HTC are 6–8 times higher than those obtained during FWC.

The heat transfer measurements at varying vapor velocity are presented in Fig. 4. The values measured for the three different surface inclinations refer to average inlet steam velocities from 3.3 to 13.8 m s^{-1}, obtained by varying the power of the resistances installed in the boiling chamber from 1 to 4 kW. As reported in Table 1, the other experimental conditions were maintained constant. In particular, the measurements were performed at constant saturation temperature (≈107 °C) and heat flux (≈410 kW m^{-2}). As shown in Fig. 4a, at the minimum vapor velocity, when varying inclination from vertical to horizontal, the HTC is reduced from 97 to 60 kW m^{-2} K^{-1}, which corresponds to a heat transfer penalization of about 40 %. As the average inlet steam velocity increases by 4 times (from 3.3 to 13.8 m s^{-1}), the HTC increases for all the surface inclinations, but at a different rate, reaching almost the same value of HTC at the highest steam velocity. Considering the vertical and 45° inclined surfaces, the HTC increases by 21 % (from 97 to 118 kW m^{-2} K^{-1}) and by 28 % (from 90 to 114 kW m^{-2} K^{-1}), respectively. Instead, for the horizontal surface, the heat transfer enhancement due to the effect of steam velocity is more pronounced: the HTC increases from 60 to 114 kW m^{-2} K^{-1} (+90 %). Considering that the HTC is found to increase with vapor velocity (Fig. 4a), whereas the heat flux q remains almost constant at 405 kW m^{-2} (Fig. 4b), the wall subcooling ΔT decreases (Fig. 4c). Since the HTC during dropwise condensation is independent from the wall subcooling in the range here investigated 3–10 K (Fig. 3), the HTC variations reported in Fig. 4a are due to the effect of steam velocity.

It must be pointed out that, after a certain value of average inlet vapor velocity (in the range 8–11 m s^{-1}), the HTC penalization associated to the horizontal surface is drastically reduced and the heat transfer performance is nearly independent from surface inclination (Fig. 4a). This can be explained looking at Fig. 5. At low vapor velocities, on the vertical and inclined surfaces, the gravity force acting on drops is mainly responsible for condensate removal. On the horizontal surface, the gravity force is perpendicular to the surface and, thus, only the vapor drag force contributes to the condensate removal. Since the drag force due to the vapor flow is weak at low vapor velocities, the drops on the horizontal surface grow to a larger size before sliding and the sweeping mechanism is less efficient, thus penalizing the HTC. Since the drag force increases with the square of the steam velocity, at v_v = 11 m s^{-1} the effect of the drag force is high enough to guarantee an efficient droplets removal, comparable to those achieved by the combined effect of gravity and drag forces in the case of the vertical and 45° inclined surfaces.

At the end of each test run (when the maximum power at the boiling chamber is reached), in order to check the repeatability of the heat transfer measurements and the independence from any modifications of the coating due to possible degradation, the thermosyphon loop is brought back to the initial condition (1 kW supplied electrical power) and a verification data point is taken. It is found that the small changes observed in the contact angle values (Sec. 2.1) do not cause any measurable effect on the HTC.

3.2. Tilt angle and vapor velocity effects on the maximum droplet radius

For the study of dropwise condensation, it is important the knowledge of droplet population. In fact, the heat flux during DWC depends both on the heat exchanged by individual drops and on the drop-size density function from the nucleation radius (r_{min}) to the departing radius (r_{max}). Furthermore, understanding the series of events that occur during the droplet growth cycle (nucleation, coalescence, and departure from the surface) is essential for DWC modeling. Of particular interest is the knowledge of the characteristic time for droplet removal due to sweeping events.

A force balance between adhesion force, gravity force and vapor drag force determines the droplet departing radius [12]. The adhesion force is mainly affected by the contact angle hysteresis. The component of the gravitational force parallel to the surface depends on the droplet volume and on the surface inclination, while the drag force is proportional to the square of the vapor velocity. The contribution of gravity is maximum for the vertically oriented condensing surface, while it is zero when the surface is horizontal. Instead, being the test rig a natural convection thermosiphon (Sec. 2.2), the drag force acting on the drops is always present, but it significantly increases with the vapor velocity. According to the literature [17,19], high vapor velocities and vertical surface orientation should reduce the average drop dimensions, favouring the renewal of the surface and, thus, increasing the condensation HTC (Fig. 4).

In Fig. 5a, the measurements of droplet departing radius are plotted vs average inlet steam velocity for the three different surface inclinations (horizontal, inclined at 45°, and vertical). The investigation was performed considering the videos recorded during DWC at constant heat flux (410 kW m^{-2}) and variable average inlet vapor velocity (3.3–13.8 m s^{-1}). Each video was analysed by a home-made MATLAB® program which is able to detect the droplet dimension when the drop starts to slide (i.e., the droplet departing radius). For each operating condition, at least 15 measurements were averaged to determine the average departing radius, and the corresponding standard deviation is reported using vertical bars.

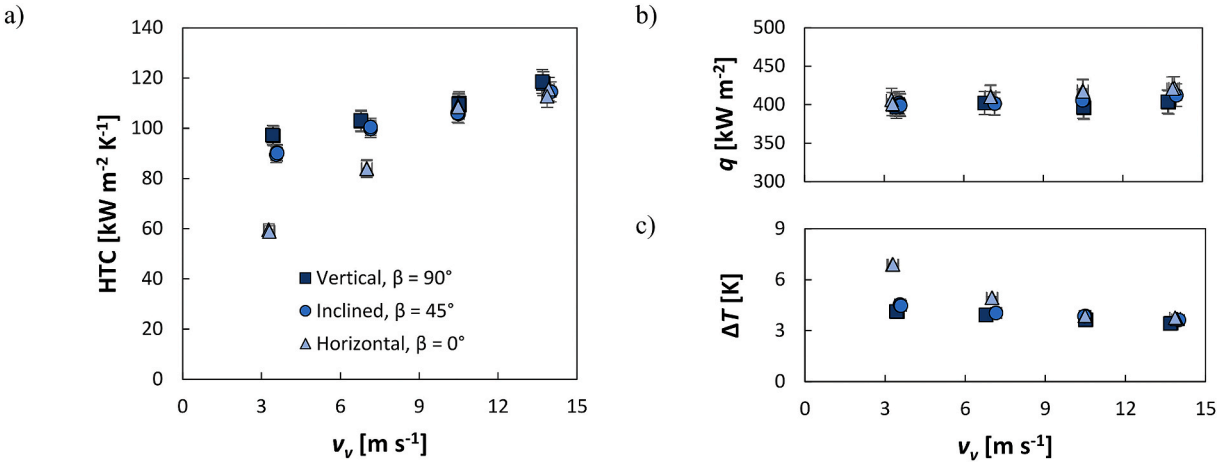

Fig. 4. Heat transfer measurements during DWC of steam at varying average inlet vapor velocity (3.4–13.8 m s^{-1}) for different inclinations of the condensing surface: vertical ($\beta = 90°$), inclined ($\beta = 45°$) and horizontal ($\beta = 0°$). (a) Heat transfer coefficient HTC, (b) heat flux q and (c) wall subcooling ΔT versus average inlet vapor velocity v_v. Values for the vertical configuration are taken from Parin et al. [20].

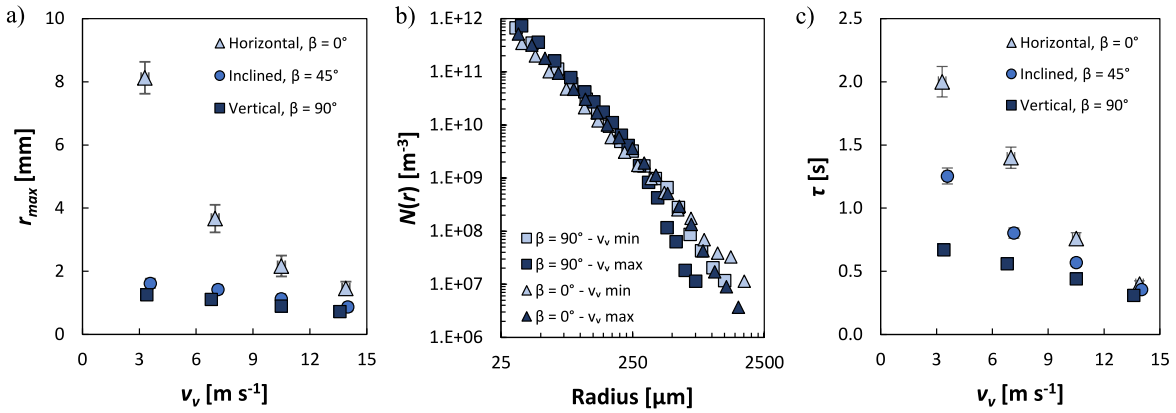

Fig. 5. Droplet population measurements for different surface inclinations. a) Droplet departing radius (r_{max}) vs average inlet vapor velocity (v_v). b) Drop-size distribution $N(r)$ evaluated on the horizontal ($\beta = 0°$) and vertical ($\beta = 90°$) surfaces at the minimum and maximum inlet vapor velocity (3.3 and 13.8 m s^{-1}) vs drop radius. c) Sweeping period (τ) vs average inlet vapor velocity. Values measured for the vertical configuration are taken by Tancon et al. [20].

Due to the absence of a component of gravity along the condensing surface, the departing radii measured on the horizontal surface were significantly larger than the values obtained on the vertical and inclined at 45° surfaces (Fig. 5a). For the minimum vapor velocity, condition at which the drag effect due to the vapor flow is the least, the departing radius on the vertical, inclined at 45° and horizontal surfaces were equal to 1.3 mm, 1.6 mm and 8.1 mm, respectively. As the average inlet steam velocity increases from 3.3 to 13.8 m s^{-1}, the drag force of the vapor increases and the average droplet size results to decrease for all the three surface inclinations (Fig. 6). In particular, the departing radius on the vertical and inclined at 45° surfaces decreases by about 45 %, from 1.3 to 0.7 mm and from 1.6 to 0.9 mm, respectively. Instead, the departing radius on the horizontal surface is reduced by 82 % (from 8.1 to 1.4 mm). Furthermore, video analysis allows to make two other observations. First, the droplet shape is nearly circular regardless of surface inclination and flow velocity. Second, the drops that reach the departing size are located at the beginning of the condensing surface except for the horizontal configuration: in this case, in particular at low vapor velocity, the actual sliding movement starts in the second half of the surface (Fig. 6). It has been proved that enhanced shedding due to increased vapor velocity results in significant increase of HTCs for all the configurations here investigated. Nevertheless, it is worth to highlight that changing the operating conditions could bring to different conclusions. Yan et al. [38] and Zhao et al. [39] studied microscale confined condensation from both experimental and computational point of view, and in those conditions they found that promoting droplet shedding when the departing radius is around ~1 mm brings only to marginal gains in HTCs.

3.3. Statistical analysis of the droplet population at varying surface inclination and steam velocity

Since the heat flux during DWC strongly depends on the droplet population, measurements of drop-size distribution are needed to develop accurate DWC models. However, drop-size distribution measurements taken during DWC are scarce in the literature. Furthermore, the few experimental data usually refer to a limited number of operating conditions [20,28,40]. In this work, the drop-size distribution $N(r)$ was investigated at varying vapor velocity and surface inclination.

For each working condition, two high-speed videos at different magnifications were recorded using the microscopic objective (Navitar 12X Zoom Lens System) coupled with the ring-shaped LED. In order to evaluate the time-averaged drop-size distribution, a homemade MATLAB® code was used to process all the 2180 frames (which correspond to a condensation time interval of 4.36 s) extracted from each high-speed video. The detailed description of the developed software and the procedure for the evaluation of the drop-size distribution can be found in Ref. [28]. For each video frame, the MATLAB® code automatically provides the positions and

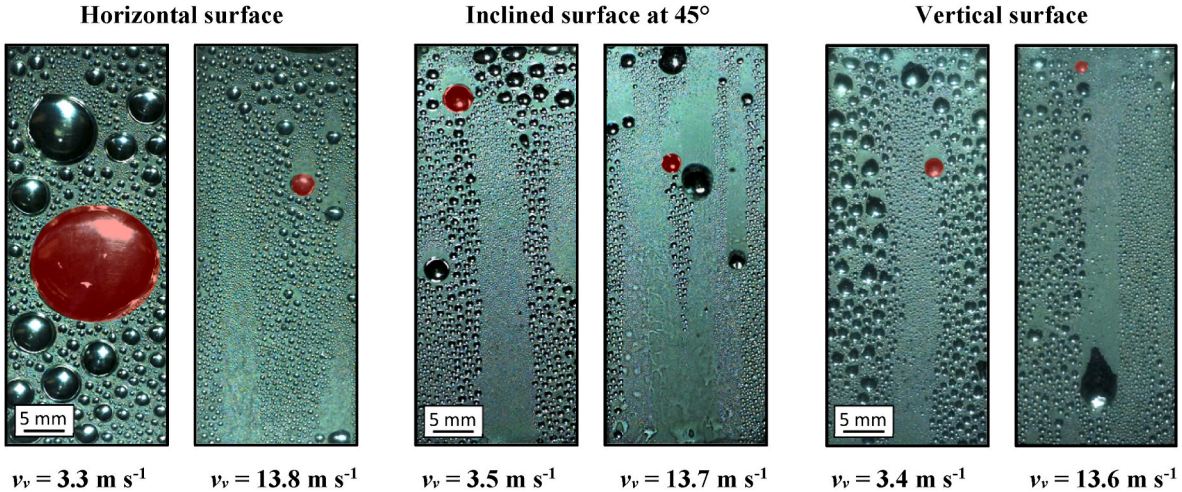

Fig. 6. Images of DWC at the minimum and maximum average inlet vapor velocity recorded for different surface inclinations considering the same area (20 mm × 50 mm). The departing droplets analysed by the software are marked with red circles.

dimensions of the drops (Fig. 7). It is worth noticing that the developed software coupled with the present experimental setup allows to map accurately the population of drops with radii larger than 25 μm. Though the following investigations are limited to those large droplets, it is important to specify the role of non-visible drops. Due to the lower thermal resistance related to the conduction through the liquid, most of the total heat flux exchanged during DWC is due to droplets with radii smaller than 10 μm. This is valid for both smooth and engineered surfaces [13,41].

Once the position and size of the droplets are automatically detected, the full range of measured drop radii is divided into multiple classes. Then, the frequency of droplet radii for each video frame is evaluated by counting each drop in a specific class according to its dimension. To obtain the average drop-size distribution, the number of droplets in a certain radius range (averaged over all the frames of a video) is divided by the investigated area and multiplied by the width of the radius range. In total, for each captured video, the drop-size distribution was evaluated by detecting an average of 5×10^5 droplets. The measurement uncertainty calculated as described in Ref. [28] is below 14 %.

Fig. 5b reports the results in terms of drop-size density (i.e., the number of drops per unit area per unit radius) for two values of surface inclination β (horizontal and vertical) and average inlet vapor velocity v_v (3.3 and 13.8 m s^{-1}). In the range of radii investigated in the present study (25–2000 μm), for all the operating conditions, the density function decreases when the radius increases. In particular, for drops with a radius smaller than few hundred micrometers, the drop-size distribution decreases following the power-law trend described in the literature [42]. Instead, because of the effect of falling droplets that clean the surface, the drop-size distribution for the larger drops (radius bigger than few hundred micrometers) shows a different slope compared to the power-law trend [20]. The larger average drop size observed in the case of the horizontally oriented sample can justify the HTC penalization shown in Figs. 3 and 4. As the average inlet steam velocity increases from 3.3 to 13.8 m s^{-1}, the average drop size diminishes for both surface inclinations. In particular, the distribution of droplets with radii in the range 25–250 μm is shifted upward by about 50 % and 15 % on the horizontal and vertical surfaces, respectively (see Fig. 10). Furthermore, the higher the vapor velocity, the higher the surface renewal rate and, thus, the smaller the number of droplets that reach the departing radius without being removed by sweeping drops. Therefore, the radius at which the drop-size distribution deviates from the power law distribution described by Le Fevre and Rose [42] is reduced.

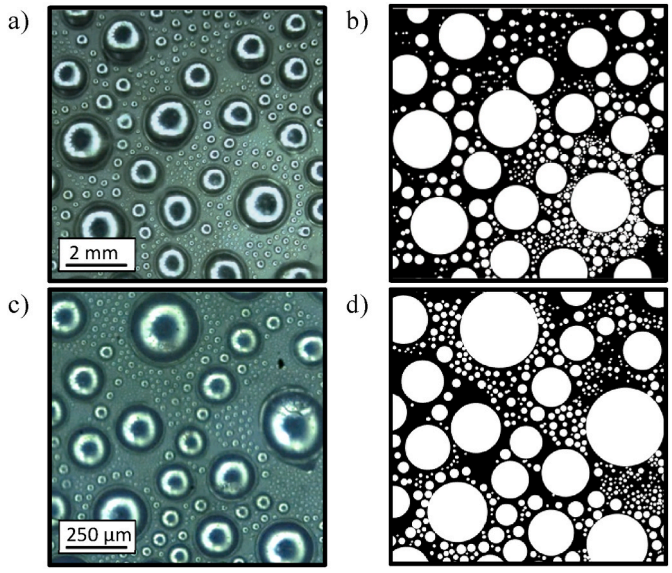

Fig. 7. a-c) Image of dropwise condensation taken by the high-speed camera coupled with a homemade ring-shape LED illumination system. b-d) Resulting reconstructed image (in black and white) obtained by the MATLAB® code.

3.4. Surface inclination and vapor velocity effects on the sweeping period

In addition to the departing radius and drop-size density, the period of the condensation cycle (which involves formation of microscopic droplets, coalescence, and departure) is an important parameter for the prediction of the heat flux during dropwise condensation. According to the population balance theory [43], the sweeping period τ (removal characteristic time) is the time necessary by large moving drops to renew the droplet population on the condensing surface. It can be evaluated as the ratio of total investigated surface (A_{tot}) to the total surface swept by falling drops within 1 s (A_{sw}).

From the macroscopic high-speed videos recorded during steady-state DWC, it was possible to evaluate the sweeping period at different average inlet vapor velocities (3.3–13.8 m s^{-1}) for the three surface inclinations here investigated. For each experimental condition, the central area of the condensing surface (1 cm × 2 cm) was considered in the analyses (Fig. S1). Considering the low renewal frequency observed in the case of the horizontal surface, especially at the minimum vapor velocity, the areas swept by all sliding drops were evaluated in a time interval of 2 s out of 3.3 s (which is the duration of each video). Then, the total investigated area was divided by the sum of the swept areas ($\sum_i A_{sw,i}$) in a certain time interval (Δt) to obtain the sweeping period ($\tau = \Delta t\, A_{tot}/\sum_i A_{sw,i}$). The procedure used to evaluate the area swept by the sliding drops is exemplified in Fig. S1.

In Fig. 5c, the sweeping period measurements are plotted versus inlet vapor velocity for the three different surface inclinations (horizontal, inclined at 45° and vertical). As the gravity contribution to the drop movement is more important at low steam velocity [19], the droplet removal frequency on the horizontal surface ($\tau = 2$ s) is much lower than those measured on the inclined at 45° surface ($\tau = 1.3$ s) and on the vertical surface ($\tau = 0.7$ s). When the average inlet vapor velocity increased from 3.3 to 13.8 m s^{-1}, the sweeping period decreased by about 80 % (from 2 to 0.4 s), 70 % (from 1.3 to 0.35 s) and 55 % (from 0.7 to 0.3 s) on the horizontal, inclined and vertical surfaces, respectively. Despite the similar values of τ assumed at the highest vapor velocity, there are some differences in the droplet dynamics. The vertical surface is characterized by a higher number of small sliding drops, whereas the sliding drops on the horizontal surface are few but larger. Overall, the time required to renew the droplet population on the condensing surface is similar. It can be concluded that the droplet renewal efficiency at high vapor velocities is almost independent on surface inclination due to the dominance of the vapor drag effect over that of gravity.

For operating conditions and coating characteristics similar to those of the present experimental campaign, drops with radii in the range 1–100 μm are responsible for 70–80 % of the total heat exchanged during dropwise condensation of pure steam, as demonstrated in Refs. [12,20]. However, the reduction of the average droplet dimension (Fig. 6) and the increase in the number of small drops (Fig. 5b) can explain only partially the increase in the HTC due to vapor velocity (Fig. 4). For example, the higher HTC measured on the horizontal surface at the maximum vapor velocity (114 kW m^{-2} K^{-1}) compared to the value measured on the vertical surface at the minimum vapor velocity (97 kW m^{-2} K^{-1}) cannot be explained only looking at the average droplet dimension. Otherwise, one might expect similar HTCs for the two considered conditions which are characterized by similar values of departing radius and drop-size distribution. Actually, there are differences in the droplet dynamics: the surface renewal mechanism due to sliding drops is more efficient at high vapor velocity as shown in Fig. 5c. The lower the sweeping period, the higher the surface renewal frequency and, thus, the higher the values of HTC. With regards to the previous two conditions, the sweeping period is equal to 0.4 s in the case of the horizontal surface at the maximum vapor velocity and 0.7 s in the case of the vertical surface at the lowest vapor velocity.

4. A computational procedure for HTC prediction accounting for surface inclination and steam velocity

The most common approach to predict the heat flux during DWC is based on the combination of the heat flow rate through a single drop with the drop size distribution function, which aims to describe the droplet population on the condensing surface. In particular, the steady-state heat flux transferred during DWC can be expressed as:

$$q = \int_{r_{min}}^{r_e} Q_d(r)\, n(r)\, \mathrm{d}r + \int_{r_e}^{r_{max}} Q_d(r)\, N(r)\, \mathrm{d}r \tag{11}$$

where $N(r)$ and $n(r)$ are, respectively, the drop-size density function of large and small droplets, r_{min} is the minimum droplet radius, r_{max} is the droplet departing radius, and r_e is the effective radius, i.e. the radius separating the two populations.

In Sec. 4.1 the numerical procedure for the determination of the maximum radius r_{max} that the droplets can reach before start sliding is reported. The parameter r_{max} is needed as input for the calculation of the drop-size distribution as reported in Sec. 4.2. Finally, the procedure for the calculation of the steady-state heat flux during dropwise condensation of steam is provided in Sec. 4.3. In particular, a computational method to predict the effect of vapor velocity and surface inclination on the HTC is presented and validated against experimental data in Sec. 4.4.

4.1. New procedure for the calculation of the maximum droplet radius r_{max}

In the literature, the departing radius is evaluated by solving the balance of the forces acting on a single drop. With regard to a droplet on a vertical surface, only two forces are usually considered: the adhesion force and the gravity force. Recently, Tancon et al. [19] proposed an analytical method for predicting the effect of steam velocity during DWC based on the contribution of drag force due to vapor flow for the calculation of r_{max}. In the present work, a step forward has been made by extending the Tancon et al. [19] model for the departing radius with different surface inclinations.

The present model for the evaluation of the departing radius is based on the assumption that droplets start to move by sliding. As previously mentioned, in the presence of non-negligible vapor velocity, the departing radius can be evaluated by equating the retentive forces (drop adhesion to the surface) and the external forces which promote drop movement (gravity and drag). The adhesion force is evaluated as:

$$F_{ad}(r) = 2\, k_c\, \sin\theta_e\ \ \sigma\, (\cos\theta_r - \cos\theta_a)\, r \tag{12}$$

where θ_r and θ_a are respectively the receding and the advancing contact angle, θ_e is the apparent equilibrium contact angle which can be evaluated as $\theta_e = \cos^{-1}(0.5\cos\theta_a + 0.5\cos\theta_r)$, σ is the surface tension of the condensing fluid and k_c is a constant (named retention factor) that depends on the drop shape. For a drop of circular shape, it is equal to $2/\pi$ [44].

The component of the gravity force parallel to the surface and acting on the drop can be evaluated as:

$$F_g(r) = \frac{2 - 3\cos\theta_e + \cos^3\theta_e}{3}\, \pi\, \rho_l\, g\, r^3\, \sin\beta \tag{13}$$

where g is the gravity acceleration and β is the tilt angle of the condensing surface from the horizontal. An angle $\beta = 90°$ corresponds to a vertically oriented condensing surface, while $\beta = 0°$ corresponds to a horizontal condensing surface.

The drag force (F_d) acting on a droplet due to the vapor velocity can be evaluated as:

$$F_d(r) = \frac{1}{2}\, \rho_v\, v_{v,avg}^2\, C_d\, (\theta_e - \sin\theta_e\, \cos\theta_e)\, r^2 \tag{14}$$

where ρ_v is the vapor density, $v_{v,avg}$ is the average vapor velocity along the sample length, θ_e is the equilibrium contact angle expressed in radians and C_d is the drag coefficient. Since the drops that reach the departing size are not always located at the beginning of the condensing surface (see video analysis in Sec. 3.2), an average value of vapor velocity along the sample length $v_{v,avg}$ has been considered as model input. The drag coefficient can be expressed as a function of two dimensionless groups, namely the ratio of the channel height to the droplet height (L_{ch}/l_{dr}) and the droplet's Reynolds number ($\mathrm{Re}_{dr} = l_{dr}\, v_v\, \rho_v/\mu_v$), as:

$$C_d = 5.6053 \left[\left(\frac{L_{ch}}{l_{dr}}\right)^{-4/3} \mathrm{Re}_{dr}^{-1/6} \right] + 0.1754 \tag{15}$$

By solving the force balance between the adhesion force, the gravity force and drag force ($F_{ad} = F_g + F_d$), it is possible to obtain a new formulation of the departing radius valid for different inclinations of the condensing surface, from horizontal to vertical:

$$r_{max} = \frac{-C + \sqrt{C^2 + 4AB}}{2B} \quad \text{for } 0° < \beta \le 90° \tag{16}$$

$$r_{max} = \frac{A}{C} \quad \text{for } \beta = 0° \tag{17}$$

where the A, B and C coefficients can be calculated as:

$$A = 2\, k_c\, \sin\theta_e\ \ \sigma\, (\cos\theta_r - \cos\theta_a) \tag{18}$$

$$B = \frac{1}{3}\left(2 - 3\cos\theta_e + \cos^3\theta_e\right) \sin\beta\, \pi\, \rho_l\, g \tag{19}$$

$$C = \frac{1}{2}\, \rho_v\, v_v^2\, C_d (\theta_e - \sin\theta_e\, \cos\theta_e) \tag{20}$$

in case of horizontal surface ($\beta = 0°$), the gravity effect is null ($B = 0$) and this simplifies the expression of the departing radius from Eq. (16) to Eq. (17). For other inclinations of the condensing surface ($0° < \beta < 90°$), the term B is not null and its contribution into the force balance increases with β. In order to solve Eq. (16), an iterative procedure is required.

In Fig. 8 the measured droplet departing radii (see Sec. 3.2) are reported together predictions obtained from the new proposed model for r_{max}. The input parameters needed to apply the model are summarized in Table 2. It must be specified that, since no significant variations of the contact angles have been observed after the condensation tests (Sec. 2.1), the advancing and receding contact angles measured prior to perform the condensation tests were used as inputs for the model. Since the vapor velocity decreases along the sample as soon as condensation proceeds, we considered the arithmetic average of vapor velocity between inlet and outlet of the test section ($v_{v,avg} = v_v/2 + v_{v,out}/2$) as model input. As described in Sec. 2.2, the inlet vapor velocity (v_v) is determined by an energy balance at the boiling chamber (Eqs. (6)–(8)), while the outlet vapor velocity ($v_{v,out}$) is obtained from the vapor quality at the exit of the condensing surface $x_{v,out}$ (Eq. (9)), which in turns depends on the condensation heat flow rate (Q). Therefore, in the present case or when a direct measurement of the outlet vapor velocity is not performed, the condensation heat flow rate must be given as input to the proposed model for the calculation of r_{max} (Eqs. (16) and (17)).

In Fig. 8a, the results of the calculated droplet departing radius are plotted versus average inlet steam velocity (3.3–13.8 m s^{-1}) and compared against experimental data for the three different surface inclinations (horizontal, inclined at 45° and vertical). When the mean vapor velocity along the sample length is taken as model input (black lines), it can be noted that the model is able to accurately predict the departing radius measurements (symbols) on the vertical, inclined at 45° and horizontal surfaces. In particular, the increase of departing radius due to the reduction in the tilt angle (lower gravity force) and the decrease of departing radius due to the increase in vapor velocity

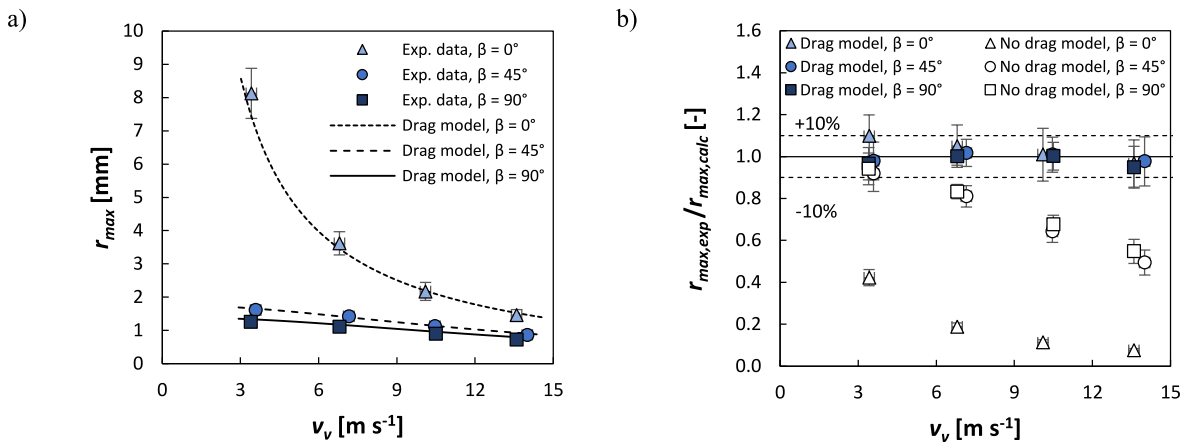

Fig. 8. a) Experimental and calculated droplet departing radius r_{max} considering the average vapor velocity along the sample length vs inlet steam velocity v_v. b) Ratio of experimental to calculated departing radius ($r_{max,exp}/r_{max,\ calc}$) vs inlet vapor velocity. Results of calculations obtained neglecting the effect of vapor drag force are also shown in the graph (empty dots).

Table 2
List of input parameters used for the evaluation of the droplet maximum radius (r_{max}), droplet distribution, and condensation heat transfer coefficient.

Parameter		Vertical surface	Inclined surface	Horizontal surface
β	[°]	90°	45°	0°
δ_{HC}	[nm]	400	400	400
λ_{HC}	[W m^{-1} K^{-1}]	0.2	0.2	0.2
T_{sat}	[°C]	107	106	107
ΔT	[K]	4.1–3.5	4.5–3.6	6.9–3.7
v_v	[m s^{-1}]	3.5–13.6	3.6–13.7	3.3–13.8
$v_{v,out}$[a]	[m s^{-1}]	1.9–12	1.9–12	1.8–12
θ_a	[°]	88	87	87
θ_r	[°]	67	64	61
N_s	[m^{-2}]	2×10^{12}	2×10^{12}	2×10^{12}

[a] Not required as input for the DWC heat transfer model.

(higher drag force) are well estimated. The average relative deviation between measurements and calculated values is below 4 %.

In Fig. 8b, the ratio of experimental to calculated droplet departing radius is plotted versus average inlet steam velocity. For comparison, the values of r_{max} predicted without considering the drag force into the force balance equation are also reported. When the drag force is not considered, to allow the resolution of the force balance equation also in the case of the horizontal surface, the tilt angle β was set equal to 0.5° instead of 0°. At the minimum vapor velocity ($v_v = 3.3$ m s^{-1}), both the models (with and without considering the drag force effect) are able to predict the departing radius with a mean relative deviation below 10 % except in the case of the horizontal surface, for which the deviation is 45 %. As the vapor velocity increases, the contribution of the drag force becomes more significant. Consequently, the deviation between measured and predicted values strongly increases for the model without considering the drag force. Instead, when the effect of the drag force is included (Eqs. (16) and (17)), the model is able to catch the decreasing trend of r_{max} with steam velocity for all the three values of tilt angle considered in the present study. In particular, the deviation between experimental and calculated values is always below 10 %. The contribution of each force acting on a droplet when it reaches the departing dimension is depicted in Fig. 9, where the values of adhesion force (in blue), gravity force (in black) and drag force (in red) are reported at varying average inlet vapor velocities (3.3–13.8 m s^{-1}) for the three different surface inclinations (vertical, inclined at 45° and horizontal). Since the adhesion force is opposing the movement of the droplet, its value is negative. As shown in Fig. 9, for a droplet at the departing radius, the force balance imposes that the sum of the gravity and drag force is always equal to the absolute value of adhesion force. The magnitude of the forces depends on the droplet size: the larger the departing radius (which is related to surface wettability and operating conditions), the higher the force required to make the droplet slide. When the steam velocity increases, for the vertical and inclined at 45° surfaces, the contribution of drag force increases in relative terms compared to the gravity force. On the other hand, for the horizontal surface, the only force acting for the droplet movement is the drag force. The results reported in Figs. 8 and 9 underline the importance of taking

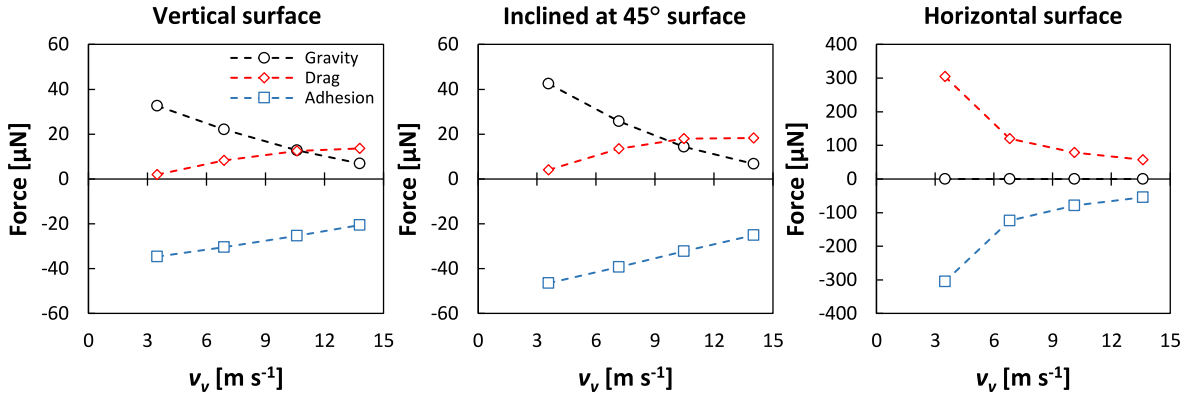

Fig. 9. Contributions due to adhesion, gravity and drag force calculated for one single drop at the departing radius when varying average inlet vapor velocity (3.3–13.8 m s^{-1}). Forces (Eqs. (12)–(14)) are calculated considering the average vapor velocity along the sample length for different surface inclinations: vertical, inclined at 45° and horizontal. The inputs for the model are reported in Table 2.

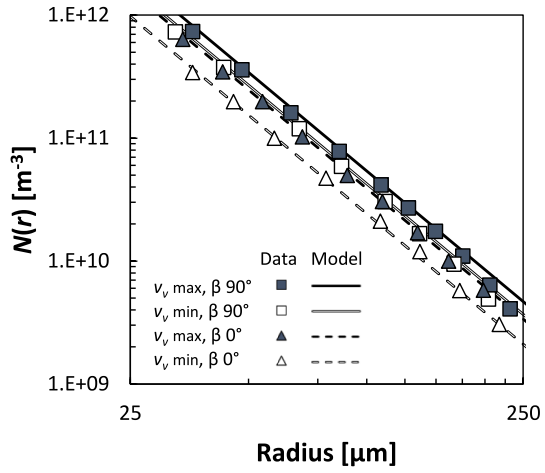

Fig. 10. Experimental drop-size distribution evaluated on the horizontal and the vertical surfaces at two different average inlet steam velocities (3.3 and 13.8 m s^{-1}) compared with the Le Fevre and Rose [42] model (Eq. (23)) coupled with Eqs. (16) and (17) for the departing radius.

into account the effect of vapor velocity on the calculation of the departing radius.

4.2. Analytical expressions for drop-size distribution

In order to calculate the total heat flux exchanged during DWC, the droplet population on the condensing surface must be determined. According to the literature [43], droplets can be classified into small droplets, whose growth mechanism is related to direct condensation of vapor, and large droplets, which grow mainly by coalescence with nearby drops. The threshold droplet dimension that separates the two droplet populations is named effective radius (r_e). The droplets with a radius between the minimum radius and the effective radius ($r_{min} \le r < r_e$) are classified as small droplets, while the drops with a radius between the effective radius and the departing radius ($r_e \le r \le r_{max}$) are classified as large drops.

Given the saturation and wall temperatures, the smallest thermodynamically stable droplet radius can be calculated from the nucleation theory [45]:

$$r_{min} = \frac{2\,\sigma\,T_{sat}}{\Delta T\,\rho_v\,h_{lv}} \tag{21}$$

If the nucleation sites are assumed randomly distributed (Poisson distribution) on the condensing surface, the effective radius (r_e) can be evaluated according to the formulation proposed by Miljkovic et al. [46]:

$$r_e = \frac{1}{4\sqrt{N_s}} \tag{22}$$

in Eq. (22) N_s is the nucleation sites density (number of nucleation sites per unit area of surface). Estimations of N_s are available in the literature: in the case of DWC of pure water vapor, the nucleation site density can be estimated between 10^9 m^{-2} and 10^{15} m^{-2} [9,47], corresponding to an effective radius smaller than 8 μm (Eq. (12)). The more appropriate choice of the N_s value will be further discussed in Sec. 4.3.

The drop-size distribution $N(r)$ of large drops can be evaluated by the semi-empirical formulation proposed by Le Fevre and Rose [42], in which $N(r)$ is a function only of the departing radius:

$$N(r) = \frac{1}{3\,\pi\,r^2\,r_{max}}\left(\frac{r}{r_{max}}\right)^{-2/3} \tag{23}$$

On the other hand, the drop-size distribution $n(r)$ of small droplets can be derived by solving the population balance theory first developed by Wu and Maa [43].

$$n(r) = N(r_e)\,\frac{r(r_e - r_{min})(A_2 r + A_3)}{r_e(r - r_{min})(A_2 r_e + A_3)}\,e^{B_1+B_2} \tag{24}$$

The main equations used to solve the distribution of small droplets and the analytical expressions for parameters A_1, A_2, A_3, B_1 and B_2, calculated as described by Miljkovic et al. [43], are reported in the Supplementary Material (Sec. S9). It is worthwhile to note that the expressions for B_1 and B_2 (Eqs. S5 and S6) include a parameter named sweeping period (τ). According to the population balance theory, the sweeping period is the removal characteristic time associated to large falling drops. Further details about the definition of sweeping period will be given in Sec. 4.4. Actually, it should be mentioned that the drop-size distribution (of both small and large drops) could also be obtained by performing numerical simulations without the need for any statistical assumption [48,49]. However, the high values of departing radius and nucleation sites density needed to simulate DWC on hydrophilic surfaces ($r_{max} \approx 1$ mm and $N_s = 10^9$-10^{15} m^{-2}) make the simulation extremely computationally expensive.

The optical technique described in Sec. 2.2 is able to accurately detect droplets with a radius higher than 25 μm. Since the effective radius (r_e) is expected to be lower than 8 μm for the investigated experimental conditions, the measured drop-size distribution will be here compared only against the model by Le Fevre and Rose [42] for the large droplet population. In particular, Eq. 23 has been coupled with the expression for departing radius proposed in Sec. 4.1 (Eq. (16) and (17)) in order to account for the effect of both vapor velocity and surface inclination on the drop-size distribution.

In Fig. 10, the measured drop-size distributions for two different average inlet vapor velocities (3.3 and 13.8 m s^{-1}) and two different inclinations ($\beta = 0°$ and $\beta = 90°$) are compared against the Le Fevre and Rose model [42] coupled with the present model for the departing radius. Since the surface renewal effect due to falling droplets changes the slope of the distribution for droplet radii near to r_{max}, (see Fig. 5b), the comparison between the experimental data and the Le Fevre and Rose model [42] is here limited to the droplets with radii from 25 to 250 μm. The model is able to accurately predict the experimental data in the whole range of droplet radii here investigated. At the minimum vapor velocity (3.3 m s^{-1}), the model can predict the droplet size increase on the horizontal surface compared to the vertical surface. In particular, due to the departing radius increase from 1.3 mm to 7.9 mm predicted by Eqs. (16) and (17) when moving from vertical to horizontal, the drop-size distribution is predicted to shift downward by about 45 % with a deviation between the experimental and the calculated values below 8 %. Furthermore, the calculation method is able to evaluate the average drop size reduction due to the increase in vapor velocity. In fact, the calculated drop-size distribution is shifted upward by about 62 % and 20 % on the horizontal and vertical surfaces, respectively, when we increase vapor velocity from 3.5 to 13.8 m s^{-1}, and the departing radius decreases as a consequence. Overall, the whole database presented in Fig. 10 is predicted with an average accuracy equal to 7 % and the maximum deviation between the experimental data and the calculated values is 22 %.

4.3. Calculation of the DWC heat flux

For the evaluation of the heat flux during DWC (Eq. (11)), the product of the heat exchanged through a single droplet (Q_{dr}) by the drop-size density function is integrated between the minimum viable droplet radius (r_{min}) and the departing droplet radius (r_{max}). In order to predict the combined effects of vapor velocity and surface inclination on the HTC, the heat flux is calculated by assembling together the procedure for the calculation of the heat transferred through a single drop proposed by Lethuillier et al. [50], the droplet population models by Miljkovic et al. [46] and by Le Fevre and Rose [42] for the distribution of small and large drops, respectively, and the expression for the droplet

departing radius (Eqs. (16) and (17)). As shown in Secs. 4.1–4.2, this expression is able to account for the effect of vapor velocity and surface inclination in the calculation of r_{max} and, when coupled with the Le Fevre and Rose [42] model, it can be also used to predict those effects on the drop-size distribution.

In the Lethuillier et al. [50] model, which is the most up-to-date model in the literature, the conduction thermal resistance within the liquid drop has been determined by numerically solving with a finite elements code the heat transfer through a single drop for the entire range of surface wettability, from superhydrophilic to superhydrophobic, and Biot numbers encountered during DWC. Since the heat flux is concentrated in the triple line region, particular attention was paid to refine the mesh in the region of the triple line to ensure the accuracy of the numerical simulations even at high Biot numbers. Hence, starting from a reference case in which the heat flux was determined analytically, the authors determined an empirical criterion on the local mesh refining needed to obtain accurate numerical results. To validate the results obtained with the finite elements code, the results were compared with a different numerical based on the Monte Carlo method. With respect to the Chavan et al. [51] model, the validity range of the Lethuillier et al. [50] model has been increased in terms of contact angles (from 20° to 170°) and Biot number (from 10^{-4} to 10^{5}).

According to Lethuillier et al. [50], the heat transfer rate Q_d through a drop having radius r is calculated with the following equation:

$$Q_d = \frac{\pi r^2 \left(1 - \frac{r_{min}}{r}\right) \Delta T}{\frac{\delta_{HC}}{\lambda_{HC} \sin^2\theta_e} + \frac{1}{2h_i(1-\cos\theta_e)} + \frac{\pi r}{\lambda_l} f(\theta_e, \mathrm{Bi})} \tag{25}$$

where h_i is the interfacial heat transfer coefficient calculated as reported in Ref. [46], considering an accommodation coefficient equal to 1 as suggested by several studies for saturated steam conditions [43,52]. In Eq. (25), the factor f depends on the equilibrium contact angle θ_e and on Biot number Bi:

$$f(\theta_e, \mathrm{Bi}) = \xi_0\ \xi_4 \quad \text{if } \mathrm{Bi} \le 10^{-2} \tag{26}$$

$$f(\theta_e, \mathrm{Bi}) = \xi_0\ [\tanh(\xi_1 - \log\mathrm{Bi}) - \tanh(\xi_2 + \xi_3 \log\mathrm{Bi}) + \xi_4\,] \quad \text{for } 10^{-2} < \mathrm{Bi} \le 10^{5} \tag{27}$$

where:

$$\xi_i = \sum_{j=0}^{6} a_{i,j}\, \theta_e^j + b_i \tan\frac{\theta_e}{2} \tag{28}$$

Coefficients $a_{i,j}$ and b_i are reported [50].

It should be noted that, since the proposed expression for r_{max} is here used together with a DWC heat transfer model, the condensation heat flow rate (Q) is no longer needed as model input. In fact, the condensation heat flux required to evaluate the average vapor velocity (which is needed in Eq. (14)) is a result of the heat transfer model (Eq. (11)). Therefore, by implementing an iterative procedure, it is first possible to solve Eqs. (16) and (17) assuming a guess value for r_{max} based on the inlet vapor velocity. With this initial value of the radius, the droplet population and heat transfer models are solved to obtain a first estimation for the DWC heat flux (q). By performing a second iteration, the vapor velocity at the exit of the condensing surface is estimated from the heat flux previously calculated, and Eqs. (16) and (17) are solved by considering the average vapor velocity along the sample length. Then, the other equations are solved and an updated value for the heat flux q is obtained. As a convergence criterion, the calculation stops when the variation of the heat transfer rate between two consecutive iterations is lower than 10^{-3} W.

4.4. Comparison of predicted HTCs against the experimental database

In the following analysis, the calculation method here proposed (Lethuillier et al. [50] model for the heat transfer through a single drop (Eq. (25)), the droplet population models by Miljkovic et al. [46] (Eq. (24)) and by Le Fevre and Rose [42] (Eq. (23)), the present model for the departing radius (Eqs. (16) and (17))) is used to predict the heat transfer coefficient data. For validation purposes, the developed calculation method has been compared against the HTC database presented in Sec. 3.1, which consists of the present data acquired on the horizontal and inclined at 45° samples, plus the measurements obtained by Parin et al. [28] and by Tancon et al. [20] on the vertically oriented substrate. The experimental data refer to heat flux in the range 260–610 kW m^{-2} and average inlet steam velocity in the range 3.3–13.8 m s^{-1} (Table 1). In Figs. 11 and 12, the predicted values of HTC obtained using the model inputs reported in Table 2 have been compared against the experimental data. It is worth providing two clarifications regarding the model inputs. First, for the evaluation of the coating thermal resistance in Eq. (25), a conductivity of 0.2 W m^{-1} K^{-1} has been assumed as reported in Sec. 2.1. The nucleation site density N_s strongly influences the heat flux during DWC. A wide range of N_s values is found in the literature [9,47]. However, since the nucleation sites density is very difficult to be measured, it has to be assumed. For DWC of pure steam over flat surfaces under thermodynamic conditions similar to those of the present study, N_s usually ranges from 10^{10} m^{-2} to 10^{15} m^{-2} [37,47]. Lower values of N_s are usually due to the presence of non-condensable gases. Here, a value of nucleation sites density N_s equal to 2×10^{12} m^{-2} was chosen for the best fitting of the experimental HTC at the lowest vapor velocity. This value of N_s is consistent with measurements found in the literature [52,53] and with assumptions made in our previous works [20,28].

In Fig. 11, the heat transfer coefficients calculated by the proposed method (lines) are compared against the experimental results (symbols) at varying heat flux (reported in Fig. 3) and vapor velocity (reported in Fig. 4) obtained with the three different surface orientations: horizontal ($\beta = 0°$), inclined at 45° ($\beta = 45°$) and vertical ($\beta = 90°$). As shown in Fig. 11a, for the lowest average inlet steam velocity (about 3.3 m s^{-1}), the present calculation method is able to accurately predict the flat trend of heat transfer coefficient with heat flux and the variation of HTC due to surface inclination. The mean deviation between predicted and measured values is lower than 3 %. Furthermore, Fig. 11b shows that the proposed method can also predict the HTC increase due to vapor velocity. In particular, the model accurately predicts the HTC augmentation in the case of the vertical and inclined at 45° surfaces, with a deviation between the calculated and the experimental values always lower than 5 %. Instead, for the horizontal condensing surface, the values of HTC at high vapor velocity ($v_v > 10.5$ m s^{-1}) are predicted with less accuracy. In fact, in this case, the maximum deviation between the predictions and the experimental data is 14 %. The droplet dynamics may suggest an explanation of this divergence. As shown in Secs. 3.2 and 3.4, the droplet dimensions and the sweeping period (i.e., surface renewal characteristic time due to sliding drops) increase when the surface inclination is moved from the vertical inclination to the horizontal, while both are reduced as the steam velocity increases. As shown in Secs. 4.1–4.2, the developed numerical method is able to predict the variation of droplets dimensions due to vapor velocity and surface inclination. However, differently from the experimental observation, this method for the evaluation of the HTC, as well as all the other DWC models in the literature [29,46], predicts a constant value of sweeping period τ. According to the population balance theory [43], the sweeping period equation (Eq. S7) depends on the equilibrium droplet radius (thus on the nucleation sites density), the minimum droplet radius (thus on the wall subcooling), the surface wettability and the coating thermal resistance. Instead, its expression does not account for the maximum droplet radius and, therefore, the sweeping period is independent from surface inclination and vapor velocity. Furthermore, recent research has shown two other critical aspects related to the sweeping period considered in the population balance theory [54]. First, the assumption of a constant removal characteristic time τ, regardless of droplet size, may not be accurate. Second, sweeping is not the only mechanism

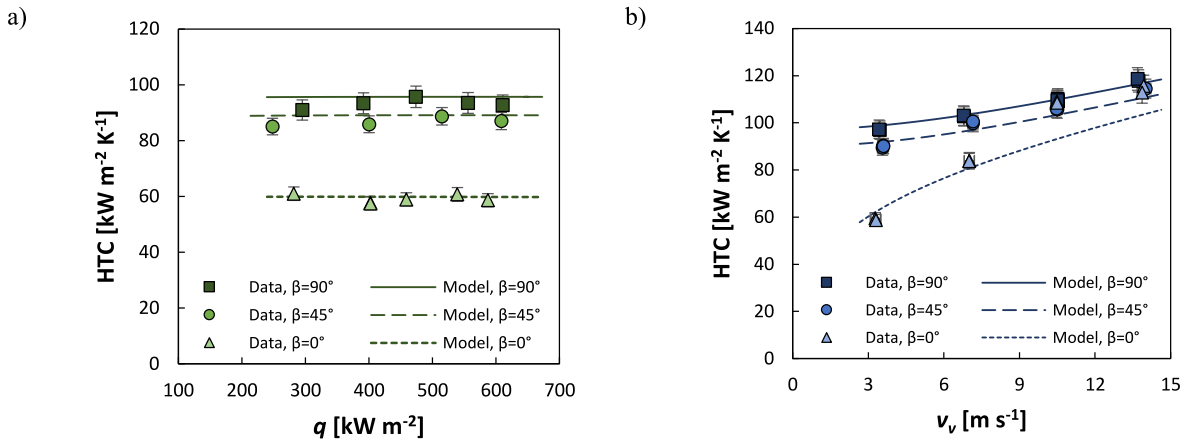

Fig. 11. Experimental data presented in Sec. 3.1 taken at different surface inclinations (horizontal $\beta = 0°$, inclined $\beta = 45°$, vertical $\beta = 90°$) and compared with predictions by the proposed calculation method. a) Experimental (symbols) and calculated (lines) HTCs versus heat flux q. b) Experimental (symbols) and calculated (lines) HTCs versus average inlet vapor velocity v_v.

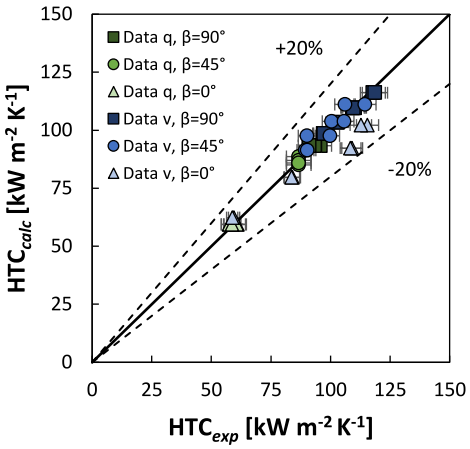

Fig. 12. Comparison between present HTC measurements obtained with different surface inclinations (horizontal $\beta = 0°$, inclined $\beta = 45°$, vertical $\beta = 90°$) and predictions by the proposed calculation method considering $N_s = 2 \times 10^{12}$ m^{-2}. Experimental data refer to heat flux in the range 260–610 kW m^{-2} (green symbols) and average inlet vapor velocity in the range 3.3–13.8 m s^{-1} (blue symbols).

involved in surface renewal, as coalescence among non-sliding drops also seems to play a major role. Actually, accounting for both the sweeping of large sliding drops and coalescence among non-sliding drops, the characteristic removal time in Eq. (24) is improperly named "sweeping period". Therefore, the sweeping period included in the model for drop-size density distribution has a different meaning than the parameter evaluated in Sec. 3.4, which instead represents the characteristic removal time due only to sliding drops. In light of these considerations, measurements of sweeping period were not included in the drop-size distribution model. However, improving the population balance theory may be a future objective for research.

Nevertheless, the proposed method has been proven to provide satisfactory predictions of the DWC heat transfer coefficient in the range of experimental conditions here investigated, even at high vapor velocity with horizontal surface inclination. Overall, the mean deviation between measurements and predicted values is 3 %, while the maximum relative deviation is equal to 14 % (Fig. 12). Finally, it is important to clarify how much the proposed calculation method is affected by the specific value assumed for N_s (2×10^{12} m^{-2}). An ad-hoc discussion is reported in the Supplementary Material (Sec. S10) considering the lower and upper limits of the nucleation sites density range: $N_s = 10^{10}$ m^{-2} and $N_s = 10^{15}$ m^{-2}. The results show that, for a nucleation sites density of 10^{15} m^{-2}, the HTC is overestimated on average by about 12 %. On the contrary, considering $N_s = 10^{10}$ m^{-2}, the calculation method leads to an average HTC underestimation by 23 %. The limited dependence of the HTC predictions on the N_s choice confirms the reliability of the proposed calculation method.

5. Conclusions

The combined effects of surface inclination (vertical, inclined at 45°, horizontal) and average inlet vapor velocity (3.3–13.8 m s^{-1}) on dropwise condensation heat transfer, droplets removal and population have been experimentally investigated in a wide range of heat flux (260–610 kW m^{-2}) on sol-gel silica-based coated aluminum samples ($\theta_a \approx 87°$, $\theta_r \approx 64°$). The results have been compared against a calculation method developed to predict the DWC heat transfer coefficient in the presence of steam velocity on surfaces with inclinations spanning from vertical downflow to horizontal ($0° \leq \beta \leq 90°$). The main results are listed here below.

- At the lowest vapor velocity (≈3.5 m s^{-1}), the HTCs measured on the inclined surface at 45° and on the horizontal specimen were respectively lower by 10 % and by 40 % compared to the vertical surface (94 kW m^{-2} K^{-1}). Due to the lower contribution of the gravity force on droplets removal, the average droplets dimensions and the sweeping period increased the more as the surface deviates from the vertical configuration.
- As the average inlet vapor velocity increased from 3.5 to 13.8 m s^{-1}, due to the drag force of the vapor, the HTC increased for all the surface inclinations, reaching roughly the same value (around 120 kW m^{-2} K^{-1}) at the highest vapor velocity. The HTC increase was due to the reduction of the average droplet size but also to the increase of the renewal efficiency, which was demonstrated to be almost independent from the surface inclination at high steam velocities.
- The model by Tancon et al. [20] for the prediction of the droplet departing radius in the presence of steam velocity has been modified to include the effect of surface inclination. The calculated values have been compared against present departing radius measurements at different average inlet vapor velocity (3.3–13.8 m s^{-1}) and surface inclination (vertical, inclined at 45° and horizontal), finding an agreement between experimental and calculated values within ±10 %.
- Droplets with radii from 20 μm to r_{max} were mapped by using an optical setup and a homemade MATLAB® program. At the lowest

vapor velocity, the drop-size density function on the horizontal surface was shifted downward by about 60 % as compared to the vertical surface. As the average inlet steam velocity increased from 3.3 to 13.8 m s^{-1}, the drop-size distribution in the range 25–250 μm was shifted upward by about 50 % and 15 % on the horizontal and vertical surfaces, respectively. The Le Fevre and Rose [42] model, coupled with the present equation for the departing radius, is able to predict the variations of $N(r)$ caused by the vapor velocity and surface inclination for droplet radii in the range 25–250 μm.

- HTC predictions obtained by coupling the Lethuillier et al. [50] model for the single droplet heat transfer, the Miljkovic et al. [46] and Le Fevre and Rose [42] droplet population models and the present equation for the departing radius have been here compared against the present HTC database, yielding satisfactory predictions of the DWC heat transfer coefficient.

Declaration of competing interest

The authors declare the following financial interests/personal relationships which may be considered as potential competing interests: Davide Del Col reports financial support was provided by European Space Agency. Corresponding author Associate Editor for International Journal of Thermal Sciences - D.D.C.

Data availability

Data will be made available on request.

Acknowledgements

The European Space Agency (France) is greatly acknowledged for supporting this work through the MAP (Microgravity Application Programme) project ENCOM-4 (AO-2004-096). The authors acknowledge the financial support of the Department of Industrial Engineering of the University of Padova through the BIRD 228237 (2022) project.

Nomenclature

A	sample area, m^2
A_{tot}	Total area investigated, m^2
A_{sw}	area swept by a falling droplet, m^2
Bi	Biot number, -
C_d	drag coefficient, -
c	specific heat capacity, J kg^{-1} K^{-1}
F	force, N
G	mass flux, kg m^{-2} s^{-1}
g	gravitational acceleration, m s^{-2}
h	specific enthalpy, J kg^{-1}
h_{lv}	latent heat of vaporization, J kg^{-1}
h_i	interfacial heat transfer coefficient, W m^{-2} K^{-1}
HTC	heat transfer coefficient, kW m^{-2} K^{-1}
k	coverage factor, -
k_c	retention factor, -
l	height, m
L_{ch}	channel height, m
$\dot{m}$	mass flow rate, kg s^{-1}
$n(r)$	small droplet population density function, m^{-3}
$N(r)$	large droplet population density function, m^{-3}
N_s	nucleation site density, m^{-2}
Q	heat flow rate, W
q	heat flux, kW m^{-2}
r	radius, m
Re	Reynolds number, -
S_v	cross section area of the test section channel, m^2
T	temperature, °C
v	velocity, m s^{-1}
x	vapor quality, -
z_1	position (1.3 mm) along z, m
z_2	position (2.8 mm) along z, m

Greek symbols

β	tilt angle between the surface and the horizontal
δ	thickness, nm
ΔT	temperature difference, K
$\Delta\theta$	contact angle hysteresis, °
θ	contact angle, °
θ_e	equilibrium contact angle, °
λ	thermal conductivity, W m^{-1} K^{-1}
μ	dynamic viscosity, Pa s
ρ	density, kg m^{-3}
τ	sweeping period, s
σ	surface tension, N m^{-1}

Subscripts

a	advancing
ad	adhesion
al	aluminum
avg	average
BC	boiling chamber
calc	calculated
d	drag
dr	droplet
e	effective
exp	experimental
g	gravity
HC	hydrophobic coating
i	position along the sample (inlet, middle, outlet)
in	test section inlet
l	saturated iquid
ls	subcooled liquid
max	maximum
min	minimum
out	test section outlet
r	receding
sat	saturation
TB	thermostatic bath (1- test section; 2- post condenser)
v	saturated vapor
vs	superheated vapor
w	water
wall	wall

Appendix A. Supplementary data

Supplementary data to this article can be found online at https://doi.org/10.1016/j.ijthermalsci.2023.108738.

References

[1] M.H. Mousa, C.M. Yang, K. Nawaz, N. Miljkovic, Review of heat transfer enhancement techniques in two-phase flows for highly efficient and sustainable cooling, Renew. Sustain. Energy Rev. 155 (2022), https://doi.org/10.1016/J.RSER.2021.111896.

[2] D.H. Nguyen, H.S. Ahn, A comprehensive review on micro/nanoscale surface modification techniques for heat transfer enhancement in heat exchanger, Int. J. Heat Mass Tran. 178 (2021), 121601, https://doi.org/10.1016/J.IJHEATMASSTRANSFER.2021.121601.

[3] D. Attinger, C. Frankiewicz, A.R. Betz, T.M. Schutzius, R. Ganguly, A. Das, C.-J. Kim, C.M. Megaridis, Surface engineering for phase change heat transfer: a review, MRS Energy Sustain. 1 (2014), https://doi.org/10.1557/mre.2014.9.

[4] S. Khandekar, K. Muralidhar, Drop Dynamics and Dropwise Condensation on Textured Surfaces, 2020, https://doi.org/10.1007/978-3-030-48461-3_5.

[5] E. Colusso, M. Tancon, L. Cazzola, R. Parin, S. Agnoli, F. De Boni, M.G. Pelizzo, E. Della Gaspera, D. Del Col, A. Martucci, Solution-processed graphene oxide coatings for enhanced heat transfer during dropwise condensation of steam, Nano Sel 2 (2021) 61–71, https://doi.org/10.1002/nano.202000105.

[6] M. Mirafiori, M. Tancon, S. Bortolin, A. Martucci, D. Del Col, Mechanisms of dropwise condensation on aluminum coated surfaces, J. Phys. Conf. Ser. 2177 (2022), 012046, https://doi.org/10.1088/1742-6596/2177/1/012046.

[7] J.M. Beér, High efficiency electric power generation: the environmental role, Prog. Energy Combust. Sci. 33 (2007) 107–134, https://doi.org/10.1016/j.pecs.2006.08.002.

[8] M.S. Patil, J.H. Seo, M.Y. Lee, M. Suresh, J.H. Seo, M.Y. Lee, Heat transfer characteristics of the heat exchangers for refrigeration, air conditioning and heap pump systems under frosting, defrosting and dry/wet conditions—a review, Appl. Therm. Eng. 113 (2017) 1071–1087, https://doi.org/10.1016/j.applthermaleng.2016.11.107.

[9] M. Tancon, M. Mirafiori, S. Bortolin, R. Parin, E. Colusso, A. Martucci, D. Del Col, Simultaneous measurement of heat flux and droplet population during dropwise condensation from humid air flowing on a vertical surface, Exp. Therm. Fluid Sci. 136 (2022), 110677, https://doi.org/10.1016/J.EXPTHERMFLUSCI.2022.110677.

[10] M. Basso, E. Colusso, M. Tancon, S. Bortolin, M. Mirafiori, M. Guglielmi, D. Del Col, A. Martucci, Hydrophobic hybrid silica sol-gel coating on aluminium: stability evaluation during saturated vapour condensation, J. Non-Cryst. Solids X 17 (2023), 100143, https://doi.org/10.1016/J.NOCX.2022.100143.

[11] A. Tripathy, K. Regulagadda, C.W.E. Lam, M.A. Donati, A. Milionis, C.S. Sharma, E. Mitridis, T.M. Schutzius, D. Poulikakos, Ultrathin durable organic hydrophobic coatings enhancing dropwise condensation heat transfer, Langmuir 38 (2022) 11296–11303, https://doi.org/10.1021/ACS.LANGMUIR.2C01477/SUPPL_FILE/LA2C01477_SI_004.MP4.

[12] S. Bortolin, M. Tancon, D. Del Col, Heat transfer enhancement during dropwise condensation over wettability-controlled surfaces, Surf. Wettability Eff. Phase Chang. (2022) 29–67, https://doi.org/10.1007/978-3-030-82992-6_3.

[13] R. Parin, M. Sturaro, S. Bortolin, A. Martucci, D. Del Col, Heat transfer during dropwise condensation of steam over a mirror polished sol-gel coated aluminum substrate, Int. J. Therm. Sci. 144 (2019) 93–106, https://doi.org/10.1016/j.ijthermalsci.2019.05.017.

[14] R. Wen, Z. Lan, B. Peng, W. Xu, X. Ma, Droplet dynamics and heat transfer for dropwise condensation at lower and ultra-lower pressure, Appl. Therm. Eng. 88 (2015) 265–273, https://doi.org/10.1016/j.applthermaleng.2014.09.069.

[15] J.Y. Ho, K.F. Rabbi, S. Khodakarami, J. Ma, K.S. Boyina, N. Miljkovic, Opportunities in nano-engineered surface designs for enhanced condensation heat and mass transfer, J. Heat Tran. 144 (2022), https://doi.org/10.1115/1.4053454/1131147.

[16] C.S. Sharma, C. Stamatopoulos, R. Suter, P.R. Von Rohr, D. Poulikakos, Rationally 3D-textured copper surfaces for laplace pressure imbalance-induced enhancement in dropwise condensation, ACS Appl. Mater. Interfaces 10 (2018) 29127–29135, https://doi.org/10.1021/acsami.8b09067.

[17] D.W. Tanner, C.J. Potter, D. Pope, D. West, Heat transfer in dropwise condensation-Part I the effects of heat flux, steam velocity and non-condensable gas concentration, Int. J. Heat Mass Tran. 8 (1965) 419–426, https://doi.org/10.1016/0017-9310(65)90005-0.

[18] I. Tanasawa, Y. Utaka, Measurement of condensation curves for dropwise condensation heat transfer, Am. Soc. Mech. Eng. Appl. Mech. Div. AMD. 30 (1979) 63–68.

[19] M. Tancon, R. Parin, S. Bortolin, A. Martucci, D. Del Col, Effect of steam velocity during dropwise condensation, Int. J. Heat Mass Tran. 165 (2021), 120624, https://doi.org/10.1016/j.ijheatmasstransfer.2020.120624.

[20] M. Tancon, M. Mirafiori, S. Bortolin, M. Basso, E. Colusso, D. Del Col, Dropwise condensation mechanisms when varying vapor velocity, Appl. Therm. Eng. 216 (2022), 119021, https://doi.org/10.1016/J.APPLTHERMALENG.2022.119021.

[21] A. Leipertz, A.P. Fröba, Improvement of condensation heat transfer by surface modifications, Heat Tran. Eng. 29 (2008) 343–356, https://doi.org/10.1080/01457630701821563.

[22] E. Citakoglu, J.W. Rose, Dropwise condensation-the effect of surface inclination, Int. J. Heat Mass Tran. 12 (1969), https://doi.org/10.1016/0017-9310(69)90045-3.

[23] R.W. Bonner, Dropwise condensation on surfaces with graded hydrophobicity, Proc. ASME Summer Heat Transf. Conf. 3 (2010) (2009) 491–495, https://doi.org/10.1115/HT2009-88516. HT2009.

[24] A. Berto, M. Azzolin, P. Lavieille, A. Glushchuk, P. Queeckers, S. Bortolin, C. S. Iorio, M. Miscevic, D. Del Col, Experimental investigation of liquid film thickness and heat transfer during condensation in microgravity, Int. J. Heat Mass Tran. 199 (2022), 123467, https://doi.org/10.1016/J.IJHEATMASSTRANSFER.2022.123467.

[25] S. Hong, J.X. Wang, Z. Gao, C. Dang, Review on state-of-the-art research in pool and flow boiling under microgravity, Exp. Therm. Fluid Sci. 144 (2023), 110848, https://doi.org/10.1016/J.EXPTHERMFLUSCI.2023.110848.

[26] A. Berto, M. Azzolin, S. Bortolin, M. Miscevic, P. Lavieille, D. Del Col, Condensation heat transfer in microgravity conditions, Npj Microgravity 9 (2023) 1–18, https://doi.org/10.1038/s41526-023-00276-1.

[27] M. Shakeri Bonab, C. Minetti, C.S. Iorio, D. Zhao, Q.S. Liu, J. Ou, R. Kempers, A. Amirfazli, Experimental investigation of dropwise condensation shedding by shearing airflow in microgravity using different surface coatings, Langmuir (2022), https://doi.org/10.1021/acs.langmuir.2c01898.

[28] R. Parin, M. Tancon, M. Mirafiori, S. Bortolin, L. Moro, L. Zago, F. Carraro, A. Martucci, D. Del Col, Heat transfer and droplet population during dropwise condensation on high durability coatings, Appl. Therm. Eng. 179 (2020), 115718, https://doi.org/10.1016/j.applthermaleng.2020.115718.

[29] S. Kim, K.J. Kim, Dropwise condensation modeling suitable for superhydrophobic surfaces, J. Heat Tran. 133 (2011) 1–8, https://doi.org/10.1115/1.4003742.

[30] H. Cha, H. Vahabi, A. Wu, S. Chavan, M.K. Kim, S. Sett, S.A. Bosch, W. Wang, A. K. Kota, N. Miljkovic, Dropwise condensation on solid hydrophilic surfaces, Sci. Adv. 6 (2020), https://doi.org/10.1126/sciadv.aax0746.

[31] A. Bisetto, S. Bortolin, D. Del Col, Experimental analysis of steam condensation over conventional and superhydrophilic vertical surfaces, Exp. Therm. Fluid Sci. 68 (2015) 216–227, https://doi.org/10.1016/j.expthermflusci.2015.04.019.

[32] R. Parin, A. Martucci, M. Sturaro, S. Bortolin, M. Bersani, F. Carraro, D. Del Col, Nano-structured aluminum surfaces for dropwise condensation, Surf. Coating. Technol. 348 (2018) 1–12, https://doi.org/10.1016/j.surfcoat.2018.05.018.

[33] J.G. (John G. Collier, J.R. Thome, Convective Boiling and Condensation, 1994, p. 596.

[34] E.W. Lemmon, M.L. Bell, I.H. Huber, M.O. McLinden, NIST Standard Reference Database 23: Reference Fluid Thermodynamic and Transport Properties-REFPROP, 2018, https://doi.org/10.18434/T4/1502528, Version 10.0.

[35] Joint Committee for Guides in Metrology, Evaluation of Measurement Data-Guide to the Expression of Uncertainty in Measurement, Sèvres, France, 2008.

[36] D. Del Col, R. Parin, A. Bisetto, S. Bortolin, A. Martucci, Film condensation of steam flowing on a hydrophobic surface, Int. J. Heat Mass Tran. 107 (2017) 307–318, https://doi.org/10.1016/j.ijheatmasstransfer.2016.10.092.

[37] J.W. Rose, Dropwise condensation theory and experiment: a review, Proc. Inst. Mech. Eng. Part A J. Power Energy. 216 (2002) 115–128, https://doi.org/10.1243/09576500260049034.

[38] X. Yan, F. Chen, C. Zhao, X. Wang, L. Li, S. Khodakarami, K. Fazle Rabbi, J. Li, M. J. Hoque, F. Chen, J. Feng, N. Miljkovic, Microscale confinement and wetting contrast enable enhanced and tunable condensation, ACS Nano 16 (2022) 9510–9522, https://doi.org/10.1021/ACSNANO.2C02669/ASSET/IMAGES/MEDIUM/NN2C02669_M005.GIF.

[39] C. Zhao, X. Yan, W. He, Z. Huang, H. Bo, F. Chen, N. Miljkovic, Exploring the limits of condensation heat transfer: a numerical study of microscale-confined condensation between parallel surfaces having wetting contrast, Int. J. Heat Mass Tran. 193 (2022), 122758, https://doi.org/10.1016/J.IJHEATMASSTRANSFER.2022.122758.

[40] J.W. Rose, L.R. Glicksman, Dropwise condensation-The distribution of drop sizes, Int. J. Heat Mass Tran. 16 (1973) 411–425, https://doi.org/10.1016/0017-9310(73)90068-9.

[41] X. Yan, F. Chen, S. Sett, S. Chavan, H. Li, L. Feng, L. Li, F. Zhao, C. Zhao, Z. Huang, N. Miljkovic, Hierarchical condensation, ACS Nano 13 (2019) 8169–8184, https://doi.org/10.1021/ACSNANO.9B03275/SUPPL_FILE/NN9B03275_SI_006.MP4.

[42] E.J. Le Fevre, J.W. Rose, A theory of heat transfer by dropwise condensation, Proc. 3rd Int. Heat Transf. Conf. 2 (1966).

[43] W.H. Wu, J.R. Maa, On the heat transfer in dropwise condensation, Chem. Eng. J. 12 (1976) 225–231.

[44] A.I. ElSherbini, A.M. Jacobi, Retention forces and contact angles for critical liquid drops on non-horizontal surfaces, J. Colloid Interface Sci. 299 (2006) 841–849, https://doi.org/10.1016/j.jcis.2006.02.018.

[45] V.P. Carey, Liquid-vapor Phase-Change Phenomena: an Introduction to the Thermophysics of Vaporization and Condensation Processes in Heat Transfer Equipment, Hemisphere Pub. Corp., Washington, D.C., 1992.

[46] N. Miljkovic, R. Enright, E.N. Wang, Modeling and optimization of superhydrophobic condensation, J. Heat Tran. 135 (2013), 111004, https://doi.org/10.1115/1.4024597.

[47] A. Katselas, R. Parin, C. Neto, Quantification of nucleation site density as a function of surface wettability on smooth surfaces, Adv. Mater. Interfac. (2022), 2200246, https://doi.org/10.1002/ADMI.202200246.

[48] K.A. Stevens, J. Crockett, D. Maynes, B.D. Iverson, Simulation of drop-size distribution during dropwise and jumping drop condensation on a vertical surface: implications for heat transfer modeling, Langmuir 35 (2019) 12858–12875, https://doi.org/10.1021/acs.langmuir.9b02232.

[49] P. Birbarah, S. Chavan, N. Miljkovic, Numerical simulation of jumping droplet condensation, Langmuir 35 (2019) 10309–10321, https://doi.org/10.1021/acs.langmuir.9b01253.

[50] J. Lethuillier, M. Miscevic, P. Lavieille, S. Blanco, C. Coustet, F. Topin, Comprehensive correlation for the prediction of the heat transfer through a single droplet in dropwise condensation regime, Appl. Therm. Eng. 209 (2022), 118233, https://doi.org/10.1016/j.applthermaleng.2022.118233.

[51] S. Chavan, H. Cha, D. Orejon, K. Nawaz, N. Singla, Y.F. Yeung, D. Park, D.H. Kang, Y. Chang, Y. Takata, N. Miljkovic, Heat transfer through a condensate droplet on hydrophobic and nanostructured superhydrophobic surfaces, Langmuir 32 (2016) 7774–7787, https://doi.org/10.1021/acs.langmuir.6b01903.

[52] C. Graham, P. Griffith, Drop size distributions and heat transfer in dropwise condensation, Int. J. Heat Mass Tran. 16 (1973) 337–346, https://doi.org/10.1016/0017-9310(73)90062-8.

[53] I. Tanasawa, J.W. Westwater, What we don'T know about the mechanism of dropwise condensation, Int. Heat Transf. Conf. 5 (2019) 186–191, https://doi.org/10.1615/ihtc5.3910.

[54] J. Lethuillier, P. Lavieille, M. Miscevic, About the role of falling droplets' sweeping in surface renewal during dropwise condensation, Langmuir 36 (2020) 12877–12886, https://doi.org/10.1021/acs.langmuir.0c02092.